

# NAVAL POSTGRADUATE SCHOOL MONTEREY, CALIFORNIA



## THESIS

### SPACE TETHER - RADAR DATA PROCESSING

By

Wayne Allan Brewster

September, 1994

Thesis Co-Advisor:

Richard C. Olsen  
Ralph Hippenstiel

**Approved for public release; distribution is unlimited.**



| REPORT DOCUMENTATION PAGE   |  |   | Form Approved OMB No. 0704-0188                     |  |
|---|--|---|---|--|
| Public reporting burden for this collection of information is estimated to average 1 hour per response, including the time for reviewing instruction, searching existing data sources, gathering and maintaining the data needed, and completing and reviewing the collection of information. Send comments regarding this burden estimate or any other aspect of this collection of information, including suggestions for reducing this burden, to Washington Headquarters Services, Directorate for Information Operations and Reports, 1215 Jefferson Davis Highway, Suite 1204, Arlington, VA 22202-4302, and to the Office of Management and Budget, Paperwork Reduction Project (0704-0188) Washington DC 20503.   |  |   |   |  |
| 1. AGENCY USE ONLY (Leave blank)  |  | 2. REPORT DATE<br>September 1994                        | 3. REPORT TYPE AND DATES COVERED<br>Master's Thesis |  |
| 4. TITLE AND SUBTITLE<br>SPACE TETHER - RADAR DATA PROCESSING   |  |   | 5. FUNDING NUMBERS                                  |  |
| 6. AUTHOR(S) Brewster, Wayne A.   |  |   |   |  |
| 7. PERFORMING ORGANIZATION NAME(S) AND ADDRESS(ES)<br>Naval Postgraduate School<br>Monterey CA 93943-5000   |  |   | 8. PERFORMING ORGANIZATION REPORT NUMBER            |  |
| 9. SPONSORING/MONITORING AGENCY NAME(S) AND ADDRESS(ES)   |  |   | 10. SPONSORING/MONITORING AGENCY REPORT NUMBER      |  |
| 11. SUPPLEMENTARY NOTES The views expressed in this thesis are those of the author and do not reflect the official policy or position of the Department of Defense or the U.S. Government.  |  |   |   |  |
| 12a. DISTRIBUTION/AVAILABILITY STATEMENT<br>Approved for public release; distribution is unlimited.   |  |   | 12b. DISTRIBUTION CODE<br>A                         |  |
| 13. ABSTRACT (maximum 200 words)<br>NASA conducted the Delta-PMG tethered satellite mission. It was conducted to verify the hollow cathode plasma source's ability to couple electric currents from each end of a long wire tether traversing the ambient low earth orbit ionosphere plasma. Observations were obtained through a suite of sensors which included large ground based VHF radars. The goal of this thesis was to process the radar data received at the radar based in Hawaii to study disturbances in the Earth's ionosphere caused by the tether. After extensive analysis, unique radar returns were identified that were associated with the passage of the tether system through magnetic field lines threading the radar's field of view. These returns were interpreted as a plasma cloud propagating along a magnetic field line and reflecting back along another. This phenomenon produced dual returns with inverted Doppler frequency content. |  |   |   |  |
| 14. SUBJECT TERMS Delta - PMG, Radar Data Processing, Plasma Cloud  |  |   | 15. NUMBER OF PAGES 81                              |  |
|   |  |   | 16. PRICE CODE                                      |  |
| 17. SECURITY CLASSIFICATION OF REPORT<br>Unclassified   | 18. SECURITY CLASSIFICATION OF THIS PAGE<br>Unclassified | 19. SECURITY CLASSIFICATION OF ABSTRACT<br>Unclassified | 20. LIMITATION OF ABSTRACT<br>UL                    |  |

Approved for public release; distribution is unlimited.

SPACE TETHER - RADAR DATA PROCESSING

by

Wayne A. Brewster  
Lieutenant Commander, Canadian Forces  
B.Eng., Royal Military College of Canada, 1984

Submitted in partial fulfillment  
of the requirements for the degrees of


**MASTER OF SCIENCE IN ELECTRICAL ENGINEERING**  
**MASTER OF SCIENCE IN APPLIED PHYSICS**

from the

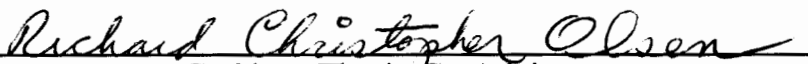
**NAVAL POSTGRADUATE SCHOOL**

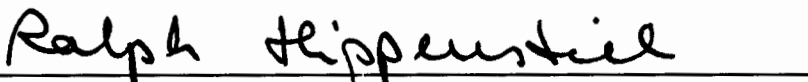
**September, 1994**

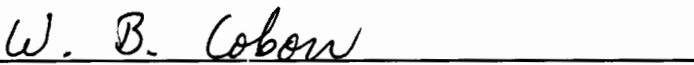
Author:

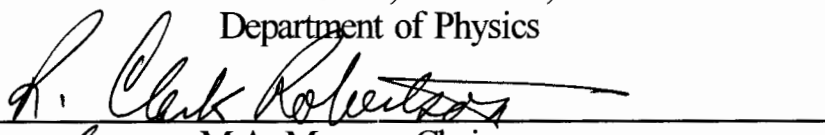
  
Wayne A. Brewster

Approved by:

  
R.C. Olsen Thesis Co-Advisor

  
R. Hippenstiel Thesis Co-Advisor

  
W.B. Colson, Chairman,  
Department of Physics

  
*for* M.A. Morgan, Chairman,  
Department of Electrical  
and Computer Engineering

## ABSTRACT

NASA conducted the Delta-PMG tethered satellite mission. It was conducted to verify the hollow cathode plasma source's ability to couple electric currents from each end of a long wire tether traversing the ambient low earth orbit ionosphere plasma. Observations were obtained through a suite of sensors which included large ground based VHF radars. The goal of this thesis was to process the radar data received at the radar based in Hawaii to study disturbances in the Earth's ionosphere caused by the tether. After extensive analysis, unique radar returns were identified that were associated with the passage of the tether system through magnetic field lines threading the radar's field of view. These returns were interpreted as a plasma cloud propagating along a magnetic field line and reflecting back along another. This phenomenon produced dual returns with inverted Doppler frequency content.

## TABLE OF CONTENTS

|  |    |
|--|----|
| I. INTRODUCTION .....                      | 1  |
| II. BACKGROUND .....                       | 2  |
| A. PLASMA MOTOR GENERATOR EXPERIMENT ..... | 2  |
| B. IONOSPHERE .....                        | 4  |
| C. TETHERS .....                           | 6  |
| D. RADAR .....                             | 11 |
| III. PROBLEM .....                         | 20 |
| A. PROCESSING .....                        | 22 |
| IV. OBSERVATIONS .....                     | 26 |
| A. PASS ONE .....                          | 26 |
| B. PASS TWO .....                          | 30 |
| V. POST ANALYSIS .....                     | 31 |
| VI. CONCLUSIONS .....                      | 35 |
| APPENDIX. PROGRAMS .....                   | 65 |
| LIST OF REFERENCES .....                   | 71 |
| INITIAL DISTRIBUTION LIST .....            | 73 |

## LIST OF FIGURES

|   |    |
|---|----|
| 1. Electrodynamic Tether Principle .....  | 37 |
| 2. PMG Hollow cathode Assembly .....  | 38 |
| 3. Typical Ionospheric Electron Density Profiles .....                                | 39 |
| 4. Radar Cross Section vs. Wavelength .....   | 40 |
| 5. TSS-1 Conducting Tether .....  | 41 |
| 6. Forces on Tethered System .....  | 42 |
| 7. Phantom current Loop .....   | 43 |
| 8. Basic radar Block Diagram .....  | 44 |
| 9. Digital Pulse Train and Fourier Transform .....                                    | 45 |
| 10. General MTI Receiver .....  | 46 |
| 11. Phased Array Antenna System .....   | 47 |
| 12. Meteor - Power Detector Output .....  | 48 |
| 13. Meteor - Range Gates vs. Time and Spectrogram .....                               | 49 |
| 14. Plasma - Power Detector Output .....  | 50 |
| 15. Plasma - Range Gates vs. Time and Spectrogram .....                               | 51 |
| 16. Autocorrelation Function - Meteor and Plasma .....                                | 52 |
| 17. Spectrogram and Autocorrelation Function,<br>Pass 1, Range Gate 16, Min. 52 ..... | 53 |
| 18. Spectrogram and Autocorrelation Function,<br>Pass 1, Range Gate 17, Min. 52 ..... | 54 |
| 19. First 16 Range Gates vs. Time, Pass 1, Min. 53 .....                              | 55 |
| 20. Spectrogram and Autocorrelation Function,<br>Pass 1, Range Gate 5, Min. 53 .....  | 56 |
| 21. Spectrogram and Autocorrelation Function,<br>Pass 1, Range Gate 6, Min. 53 .....  | 57 |
| 22. Spectrogram and Autocorrelation Function,<br>Pass 1, Range Gate 9, Min. 53 .....  | 58 |
| 23. Spectrogram and Autocorrelation Function,<br>Pass 1, Range Gate 22, Min. 56 ..... | 59 |
| 24. First 16 Range Gates vs. Time, Pass 1, Min. 58 .....                              | 60 |
| 25. Spectrogram and Autocorrelation Function,<br>Pass 1, Range Gate 3, Min. 58 .....  | 61 |
| 26. Spectrogram and Autocorrelation Function,<br>Pass 1, Range Gate 6, Min. 58 .....  | 62 |
| 27. Spectrogram and Autocorrelation Function,<br>Pass 2, Range Gate 4, Min. 34 .....  | 63 |
| 28. Spectrogram and Autocorrelation Function,<br>Pass 2, Range Gate 19, Min. 37 ..... | 64 |

## ACKNOWLEDGMENTS

I would like to acknowledge my thesis advisors, Professor Olsen and Professor Hippenstiel, for their support and guidance. Their expertise has proven invaluable to me throughout the writing of this thesis. I would also like to express my gratitude to Dr. Jerry Jost and Dr. Jim McCoy for their roles in successfully conducting the PMG experiment and providing the required information and data. Finally, I would like to thank Professor Gnanalingam, his expertise was surely needed and greatly appreciated.

## I. INTRODUCTION

An electrodynamic tether is an orbiting satellite system with two bodies or payloads connected by a conductive wire. Electrodynamic tethers make use of interactions between a moving conductor, the Earth's magnetic field and the ambient plasma in the Earth's ionosphere. These interactions can produce propulsion, braking and power generation.

The passage of the tethered satellite through the ionosphere will produce perturbations in the environment. Radio waves at the appropriate frequency will be reflected by perturbations that sufficiently increase the electron density in the ionosphere medium. Thus, a radar could be used to monitor plasma-perturbation signatures caused by a tethered satellite's movement through the ionosphere.

NASA conducted the Delta-PMG tethered satellite mission. The experiment was conducted to verify the hollow cathode plasma source's ability to couple electric currents from each end of a long wire traversing the ambient low earth orbit ionosphere plasma.

To complement the onboard data recording, ground based VHF radars were used. They provided a validation for observable interactions between the plasma motor generator system and the low earth orbit environment.

The goal of this thesis research is to process available radar data and study disturbances in the Earth's ionosphere caused by the passage of the tether.

## II. BACKGROUND

### A. PLASMA MOTOR GENERATOR EXPERIMENT

NASA conducted the Delta-PMG tethered satellite mission June 26, 1993. It was conducted in low earth orbit to confirm theoretical predictions that a low-density, weakly ionized gas from a hollow cathode assembly acting as an ionospheric plasma contactor would provide a low impedance electrical coupling between spacecraft and the ionosphere. A secondary goal was to demonstrate electrodynamic-tether behavior in low earth orbit as it functioned as either an orbit-boosting electrical motor or a generator that converts orbital energy into electricity.

The flight hardware shown in Figure 1, consisted of four major subsystems, the far end package, near end package, electronics box and the plasma diagnostic package. The system was launched piggy back on an Air Force Delta II rocket. The system was deployed with the second stage after fuel depletion and was left in an elliptical orbit. The plasma motor generator far end package was spring ejected on a 500 meter conducting wire. The two bodied tethered satellite system stabilized in a gravity-gradient configuration with the far end package above the Delta II second stage to which was attached the near end package.

The measurement plan utilized onboard telemetry data and a remote sensor suite. The remote sensors included fixed and transportable radars, magnetometers, and optical systems. The large remote sensor suite was used to observe large-scale geophysical processes, such as the electrical current coupling, far end package deployment, operation of the hollow cathode plasma sources, current flow along geomagnetic field lines and drag and thrust forces ( $\mathbf{I} \times \mathbf{B}$ ). The remote sensors also compiled data on space-based hollow cathode plasma production, tether current closure through ionosphere, tether dynamics and  $\mathbf{I} \times \mathbf{B}$  forces on the tether.

The ground based radar system used was composed of four VHF radar systems. All four systems operated in a pulsed, narrow-band, fixed-pointing configuration with a center frequency at approximately 50 MHz. The four systems were deployed at

Hawaii, Pohnpei in Micronesia, and Jicamarca and Piura in Peru. The data used for this thesis was obtained from the radar based in Hawaii.

The core hardware components were the hollow cathode assemblies. They needed to produce plasma which would couple electric currents from either end of the tether to the low earth ionosphere. Figure 1 displays the hollow cathode assembly cross section and schematic diagram. Functionally, the hollow cathode assembly heats a flow of xenon gas to approximately 1300 degrees celsius, within a barium-oxide impregnated tungsten hollow electron-emitter cathode in the presence of a strong voltage gradient between the cathode and an anode plate. In this state the gas flow is ionized by the discharge resulting in a dense plasma. This plasma can couple to the environment allowing current to flow freely between the hollow cathode and the ionosphere.

In the plasma motor generator system there were two hollow cathode assemblies with a differential voltage between them. One attached to the second stage of the Delta II rocket as part of the near end package and one deployed at the end of the 500 meter conducting tether as part of the far end package. The current loop was composed of the space plasma, the far end package, tether, load, battery, near end package including second stage rocket body and back to the plasma. The current through the tether was the net effect of current flow through both plasma clouds to their respective local space plasma environments and the current collected directly by exposed conducting surfaces of the system. The exposed conducting surfaces of the system were mainly the second stage rocket body. One of the hollow cathode assemblies acted as a collector of electrons and the other acted as an emitter of electrons. The two possible arrangements of this system and their respective interactions with the ionosphere are shown in Figure 1. The first arrangement is when the electrons are collected at the far end package which places the plasma motor generator system in the motor mode. The second arrangement is when the electrons

are collected at the near end package and the system is in the generator mode. The modes refer to how the geomagnetic field interacts with the tethered system.

The useful experiment duration was six to seven hours, which corresponds to the life expectancy of the onboard batteries. This time allowed for approximately four orbits and allowed ground based sites to collect data during at least three passes.

## **B. IONOSPHERE**

The earth's upper atmosphere, extending from 60 to 1000 kilometers is called the Ionosphere. The ionosphere contains free electrons and ions in sufficient numbers to influence the propagation of electromagnetic radiation. The electron density is distributed in a series of layers. The different layers are produced primarily by the photoionization of various atmospheric gases by diverse wavelengths of solar ultraviolet and X-ray radiation.

The ionosphere is divided into different regions which, for historical reasons have been named by letters of the alphabet. These regions are depicted in Figure 3. The D-region extends from 50 to 90 kilometers, the E-region extends from 90 to 140 kilometers and the F-region which is usually subdivided into F1 and F2 regions, extends from 140 to 1000 kilometers. The electron densities in these regions vary with time of day, season and solar activity.

Radio waves are refracted or reflected by the ionosphere. The influence of the ionosphere on radio waves decreases with increasing frequency. Waves of sufficiently high frequency can pass through hardly affected, but lower frequencies are reflected. The critical frequency is a function of electron density, frequency and angle of incidence.

For reflection of a radio wave by the ionosphere, neglecting the geomagnetic field, the following criteria must be met

$$N = [f \cos(\theta)]^2/80.6 \quad (1)$$

with  $N$  = electron density (electrons/m<sup>3</sup>);  
 $\theta$  = angle of incidence; and  
 $f$  = radio frequency (Hz).

The ionosphere can be inhomogeneous on a micro scale and have various unstable pockets that have an electron density high enough to reflect radio waves even if the average density is insufficient.

Irregular meteor arrivals, cause the most echoes, and will have many echo characteristics. The size of the meteor will determine the amount of ionization produced, the target strength and the duration of the trail. The energy developed in collisions between ablated atoms of the meteor and molecules or atoms of the upper atmosphere is sufficient to free electrons from the atoms. The electrons produce the scattering phenomena, and may conveniently be divided into two major subdivisions depending on whether the number of electrons produced per meter of path length is smaller or greater than the critical value. If smaller, the meteor trail is said to be underdense, allowing the radio wave to penetrate the column freely. Then each electron acts as an individual Rayleigh scattering source. If greater, the trail is overdense and the radio wave does not penetrate the column, but is effectively reflected as the electrons are dense enough to cause total reflection. The electron diffusion coefficient (observed decay time) depends on the atmospheric pressure and therefore on the height.

Rayleigh scattering refers to the relationship between target size, frequency of radio waves and target's effective radar cross section. The scattering cross section of a target describes and quantifies the fraction of radio frequency energy scattered back.

The quantitative study of the scattering of electromagnetic waves was preceded by the study of optics by over half a century. One concept of scattering from optics that is of relevance in radar, is the terminology which may be applied to the dimensions of a target relative to wavelength. The relationship between the radar cross section of a spherical target and its circumference measured in wavelengths is shown

in Figure 4. The magnitude of the cross section varies from virtually nothing to approximately the physical cross section. When the dimensions of the scattering object are much less than a wavelength, one refers to Rayleigh scattering. As the target size increases to where the circumference is approximately equivalent to a wavelength, then scattering becomes Mie or resonant. As the target circumference becomes larger than several wavelengths then the scattering becomes optical.

The Rayleigh scattering region is where the radar cross section is proportional to the fourth power of the frequency, is where less than critical electron density detection takes place.

The exact calculation of the scattering cross section requires the solution of Maxwell's equations, subject to appropriate boundary conditions on the surface of the scatterer.

### **C. TETHERS**

With the exception of some very far sighted astronomers doing some thought experiments, the history of tethers is a short one. The first tether concepts to be tested were during the Gemini-Agena experiment in 1966. During the flight two bodies connected by a tether were shown to have an induced angular momentum. Also it was shown that the two bodies could maintain a vertical position with the gravity gradient force pulling them apart. It was shown that in both cases there was induced artificial gravity in both of the bodies which pushed all liquids in the bodies to the farthest point from the tether.[NASA, 1986]

It was not until 1974 that Colombo, working for the Smithsonian Astrophysical Observatory, published the idea of using a tether and it's interaction with the geomagnetic field to produce thrust or propulsion.[Penzo, 1984]

#### **1. Tether Theory**

Tethers may be conducting or shielded. They generally have several different layers which provide extra strength. Figure 5 shows an example of the tether used during the TSS-1 experiment. Tether systems can be of various forms. The simplest

and most general is two masses connected by a tether. The forces acting on this system in orbit are shown in Figure 6. The main forces acting on the system are gravitational and centrifugal. The upper mass, being at a greater radius will feel a larger centrifugal force. The lower mass will feel a stronger gravitational force. The two forces are equal and balanced only at the system's center of gravity. The center of mass is in free fall as it orbits the Earth, but the two end masses are not. The tether ensures the two masses orbit at the same angular speed as the center of mass. Without the tether, the upper mass would move slower, and the lower mass would move faster than the center of mass. It is for this reason that the upper mass experiences a larger centrifugal force and the lower mass a larger gravitational force. These opposing forces give rise to the balancing tether tension and produce the restoring forces when the system is not exactly vertical. The tension acts as an artificial gravity force on the masses. This artificial gravity force or tether tension equals the gravity-gradient force. Central to tether applications and the stabilization of tethered platforms are these gravity-gradient forces.

The gravity-gradient force can be calculated by [NASA, 1986]

$$F_G = 3Lm\omega_o^2 \quad (2)$$

with  $m$  = mass;

$L$  = distance from the center of gravity; and

$\omega_o$  = orbital angular velocity ( $s^{-1}$ ).

This force is negative for a mass below the center of gravity and positive for a mass above.

The orbital speed squared of the center of gravity is given by

$$v_o^2 = GM/r \quad (3)$$

with  $M =$  mass of the Earth ( $5.979 \times 10^{24}$  Kg);

$G =$  universal gravitational constant ( $6.673 \times 10^{-11}$  Nm<sup>2</sup>/Kg<sup>2</sup>); and

$r =$  radius of the system's center of gravity from the Earth's center (m).

These forces make the vertical orientation of the tether system stable, but these are not the only forces acting on the system. Other forces include the Earth's oblateness, differential atmospheric drag due to varying air densities and electrodynamic forces. These forces are weak but persistent and cause the system to oscillate about the vertical. These oscillations have frequencies which are independent of tether length. The oscillations can be damped out by properly lengthening or shortening the tether length as a function of the tension on the tether.

## 2. ELECTRODYNAMICS

With respect to tethers, electrostatics defines the class of systems which generate any electromagnetic quantity or effect. The systems can be further subdivided into subsystems. Electrodynamic systems have moving parts within the system which generate the electromagnetic effect, and the electrostatic systems do not.

The electrostatic systems rely on the interaction of a conducting tether with the planetary magnetic field and plasma. These systems can be designed to produce either electrical power or thrust and drag.

In the electric power generator mode the tether system cuts across the geomagnetic field which induces an electromotive force across the length of the tether. The electromotive potential generated is given by

$$V = \int (\underline{v} \times \underline{B}) \cdot d\underline{l} \quad (4)$$

with  $V =$  induced electromotive potential (volts);

$\underline{v} =$  tether velocity relative to geomagnetic field; and

$\underline{B} =$  magnetic field strength (Tesla).

When the tether is vertical and ( $\underline{v} \times \underline{B}$ ) is assumed nominally vertical, this reduces to

$$V=LvB\sin(\theta) \quad (5)$$

with  $L$  = length of the tether (m);  
 $v$  = magnitude of velocity; and  
 $\theta$  = angle between  $\underline{v}$  and  $\underline{B}$ .

It can be seen that the induced electromotive potential is greatest when the tether velocity and magnetic field are perpendicular, which happens on low-inclination orbits.

Figure 2 shows how the electromotive force creates a potential difference across the tether. Since the tether travels in an easterly direction the top of the tether is made positive with respect to the lower end. This acts to collect electrons at the top end and drive them down the tether, where they are emitted.

In order for this process to work, the tether ends must make electrical contact with the Earth's plasma environment. When contact is made a "phantom loop" is produced through the tether, external plasma, and ionosphere. This closed loop path is shown in Figure 7. The free charges are constrained to move along the geomagnetic field lines traversed by the tether. They flow along one field line until they reach a point in the lower ionosphere where the charge can migrate across to the other field line, closing the circuit. The migration is accomplished by collisions with neutral particles of sufficient density.

A very important component of the tether system is the plasma contactors, which connect the system with the ionosphere. In order to operate effectively the plasma contactors must spread the tether current over a large area to reduce current densities. In this experiment the Plasma Motor-Generator used hollow cathodes as plasma contactors. The hollow cathode at each end of the tether generates an expanding cloud of highly conductive plasma. The plasma density is very high at the

tip of the tether, and falls off to ionospheric densities at a large distance from the tip. This plasma cloud produces sufficient electron density to carry the full tether current in either direction at any distance from the tether, until it is merged into the ambient ionospheric plasma currents.

The current passing through the tether can be controlled by direct current impedance matching. This is done by adjusting a continuously variable load impedance in order to match the varying tether voltage and power with the spacecraft load power requirements.

The tether may also be used to generate thrust or drag. The induced electromotive force across the tether can produce a current as discussed earlier. When this current is allowed to flow, a force is exerted on the current by the geomagnetic field. This force, for a vertical tether is given by

$$\underline{F} = I \underline{L} \times \underline{B} \quad (6)$$

By using the vector cross product this reduces to

$$F = ILB \sin(\theta) \quad (7)$$

with  $F$  = force exerted on the tether by the magnetic field;

$I$  = tether current (amps);

$B$  = magnetic field strength (webers/m<sup>2</sup>); and

$\theta$  = angle between  $\underline{L}$  and  $\underline{B}$ .

This equation states that the force is maximum when the tether is perpendicular to both the magnetic field line.

Now depending upon relative orientation the force can have components parallel and perpendicular to the velocity of the tether. The parallel component will affect the magnitude of the tether velocity. When the tether's orbital velocity is to the east and is greater than the rotational velocity of the geomagnetic field, then the force

acts as a drag. This drag force will attempt to match the tether's velocity to that of the geomagnetic field's rotational velocity.

Figure 2 shows that when current from an on-board source is fed into the tether against the induced electromotive force, the force will act as a propulsive force.

#### **D. RADAR**

The term 'Radar' is an acronym for RAdio Detection And Ranging. It was devised by the United States Navy in 1940 and officially adopted by the Allied Powers in 1943.

A radar system uses radio frequency electromagnetic waves and their reflections to provide information on the range, angle and speed of a target.

##### **1. History**

Radar as we know it today dates from the 1930's, but this was not its origin. Although, radar theory developed slowly until World War II produced a need, the basic concepts had already been discovered. The first detection of an object, using radio waves was by a German engineer, Hulsmeyer in 1903. Hulsmeyer patented the detection of radio waves reflected from ships at very short ranges. In 1925 pulses of radio frequency energy were used to measure the height of the ionosphere. The detection of aircraft was demonstrated in 1933 by the use of a continuous wave radar. This method detected the presence but not the range of the target. The first pulsed technique to detect and measure the range of an aircraft was demonstrated in 1935.[Swords, 1986]

The most significant development in radar was the magnetron. This development opened up the field to higher power microwave radars of relatively small sizes, and also made radar a more attractive commercial option.

Although most radar theory was known by the end of World War II, it was not until more recent technical advances could radar development progress. These advances included electrically steered Phased Arrays, phase stable amplifiers, digital signal processing using computers and Fast Fourier Transforms.

## **2. Theory of Operation**

The function of radar is to detect and locate targets and extract as much information about the target as possible or as defined by the mission. The majority of radars illuminate targets by transmitting bursts of energy and then listening for echoes while the transmitter is silent. This type of radar is known as a pulsed radar. There are also radars that illuminate the target area with a continuous wave and listen for echoes with a receive antenna far removed from the transmitting antenna. Radars can generally be subdivided by the type of transmitter used. The main distinctions are made by the form of illumination and if phase coherence is required on reception.

The pulsed radar in simplified form has the basic structure shown in Figure 8. The transmitter is composed of a frequency generator, a synchronizing circuit and a pulse forming network. The frequency generator is a high power radio frequency oscillator. It consists of either a non-coherent high powered magnetron which oscillates when pulsed, or a coherent low powered device that oscillates continuously with an output stage that switches the signal on and off and supplies amplification. A coherent frequency generator maintains phase from pulse to pulse, where as a non-coherent oscillator starts a new oscillation for every pulse with random phase. The synchronization circuit is responsible for coordinating the timing of the entire radar. The pulse forming network produces the pulse train as dictated by the synchronization circuit.

The antenna system is connected to the radar via a duplexer. This component enables a single antenna to be used for both receive and transmit. As dictated by the timing circuits the duplexer alters the routing of signals to protect the receiver on transmission and maximize the return echo strength when the transmitter is silent. The antenna may take on various shapes and sizes depending on the mission and the area to be illuminated by the pulse.

The receiver's main function is to amplify the received echo to the level required by the signal processing unit. The majority of the amplification is done after

the echo's frequency has been lowered to an intermediate frequency which is easier to work with. Finally the signal is processed depending upon the required information and displayed in an appropriate fashion so as to allow the operator to comprehend the data. The most common display is a cathode ray tube which is synchronized with the pulse.

The components interact to detect and locate a target in a simple manner. The synchronization and pulse forming network periodically cause the transmitter to generate a burst of electromagnetic energy. The pulse's parameters vary depending upon the desired information or mission. It is defined by the length of the pulse, the length of time between pulses and the power level. At the same time the transmission occurs, a timer is started. The energy is delivered by the duplexer to the antenna, where it is concentrated into a beam pointed in the direction the radar is searching. The concentrated energy propagates through the atmosphere at a speed near the speed of light in free space. If the wave encounters an object, a portion of the energy striking the object is reflected. The energy is reflected in many directions, but only the portion reflected directly back to the receiver is useful. The energy reflected back towards the radar is called backscatter. The backscatter energy propagates back through the atmosphere where it is intercepted by the antenna. The larger the antenna, the more backscatter energy it can intercept. The antenna also intercepts echoes from objects not desired and interfering signals, called clutter which distort the target echo. The captured energy is directed by the duplexer to the receiver, where it is amplified, filtered and reduced to a lower intermediate frequency. Unfortunately, the receiver also generates noise, which again reduces the signal to noise ratio. All these competing energies are fed to the processing unit. The processing unit works specifically to reduce the interference and enhance the target echo. The processed signals are compared to a reference level called a detection threshold and if they exceed this level then a target is deemed to be present. If the clutter and noise is sufficient to exceed the threshold then a false alarm occurs. If the target return is too small to cross the

threshold the target is missed. Detection is described statistically and radars will be described by their probability of false alarm and probability of detection. When detection occurs the timer is sampled to measure the targets round trip time for the calculation of range, and the antenna location details the angle of the target. Motion of the target with respect to the radar will cause a frequency shift in the return signal, allowing the velocity of the target to be determined from the Doppler frequency.

A radar's parameters are set depending upon the radar's task. To understand how a radar will perform, the interrelationship between all these parameters must be known. The main defining parameters are the pulse width, pulse repetition period, frequency and size and shape of the antenna.

As stated earlier, a pulsed radar sends out a train of pulses. This train of pulses is defined by the pulse width and pulse repetition period. The pulse width defines the radars range discrimination. If a second target is within the distance light can travel in one half the pulse width it will be indistinguishable from the first target. This is because the front end of the second return will overlap with the trailing edge of the first return. This is defined as the radar's range resolution. The pulse repetition period defines the radar's unambiguous range. If a targets range is such that light can not travel to the target and back again in one pulse repetition period, then the next pulse is transmitted prior to the echo returning. Thus the radar will not be able to tell if the return is from a small close target, or a large target that is far away. Depending upon atmospheric attenuation, target returns may arrive after several other pulses have been transmitted. These returns are defined as multiple time around echoes and their range is ambiguous. To fully understand the effects of the pulse width and pulse repetition period the frequency spectrum must also be considered. The pulse train and it's Fourier transform is shown in Figure 9. The main sinc function is the result of the pulsed carrier and has a width at half maximum equal to the reciprocal of the pulse width and is centered at the frequency of the transmitted wave. The pulse train produces a spectrum which is a series of sinc functions separated by one over the pulse repetition

period. Each of the underlying sinc functions have a width at half maximum of one over the pulse repetition period multiplied by the number of pulses used for the calculation of the echo's frequency content. The frequency domain spectrum allows the maximum unambiguous Doppler frequency shift to be one over twice the pulse repetition period, as any shift greater than this will result in the ambiguity of which underlying sinc function was actually shifted. The maximum frequency resolution is defined by the width at half maximum of the underlying sinc function which is given by one over the number of pulses processed multiplied by the pulse repetition period.

The choice of frequency for the radar is a function of the target's shape and size, ranges desired and the medium over which the pulse must travel. The attenuation of the medium and the targets radar cross section vary as a function of frequency. The medium through which the energy must propagate is set and charts are available that show the best part of the spectrum to use for each particular job. The way a target's size and shape affect it's radar cross section has already been discussed.

The size and shape of the antenna affect the radar by defining the shape of the beam transmitted or more directly the percentage of energy transmitted that is directed towards the target. The beamwidth is defined by diffraction as defined in

$$\theta_{1/2} = a \lambda D \quad (8)$$

with  $\lambda$  = wavelength;

$a$  = constant depending upon shape of the aperture; and

$D$  = antenna diameter in direction of interest.

The beamwidth is defined by the half angle in azimuth and elevation multiplied by the range. This in turn determines the radar's ability to discriminate targets in elevation and azimuth. These relationships cover the basic radar principles required to understand a radar system but are by no means complete.

Once the radar has received the return energy it must process it to determine if a target is present. The basic function of a receiver is to take the received energy at the transmitted frequency plus the Doppler frequency imparted by the target, amplify it and lower it to an intermediate frequency. Once at the intermediate frequency the signal can once again be amplified but since it is at a lower frequency much more amplification is possible. For radars that require Doppler information, the phase relationships must be maintained. The basic block diagram is shown in Figure 10. A coherent sample of the transmitted pulse is used to offset the echo's frequency downward. To determine the sign of the Doppler frequency the relative phase must be known. The echo's frequency is lowered using two channels and a coherent oscillator (COHO), one mixed with the coherent oscillator in phase and one with a ninety degree phase shift. This process also eliminates blind phases, which is when two different phase shifts look identical at the radar's sampling frequency. The two signals are then digitized and stored for further processing.

The simplest detection scheme is to compare the returned energy to a preset threshold and if it surpasses this preset level the presence of a target is declared. Generally more sophisticated procedures are required. For each pulse the receiver output is sampled at a preset frequency. These samples are saved as a row vector with each subsequent pulse being a new row. This is best perceived as a matrix with each row being a different pulse and each column specifying a distance from the radar. The columns are defined as range cells as the distance from the radar is not precise. The transmitted pulse has a specified width which determines the radar's range resolution. If two targets are within the distance light can travel in one pulse width, the front edge of second return will overlap the trailing edge of the first. This minimum range resolution defines the optimum sampling period and each column defines a range resolution cell. It is important to keep in mind that the composite signal samples which are processed together arrive at the radar simultaneously in time. Or

equivalently, only one range bin is analyzed at a time. This is the key concept in radar signal processing.

Since the clutter is stationary and the noise is statistically random, the processing is able to increase the signal strength with respect to the background. Random noise samples will on average cancel each other, so by adding successive pulses the signal to noise ratio will be increased. Equivalently, if the target is moving it can be separated from stationary clutter in the frequency domain by the use of a delay line canceler. This is achieved by delaying each pulse and subtracting it from the next pulse. The magnitude of the transfer function for a delay line canceler is given by

$$\|H(f)\| = \|2\sin(\pi fT)\| \quad (9)$$

With the pulse repetition period  $T$  being one over the pulse repetition frequency. In the frequency domain this lowers the level of returns with no or little Doppler shift, and is maximum at one half the pulse repetition frequency.

Finally if the signal is to be processed for Doppler information it is best done by taking the Fast Fourier Transform over a set number of samples from the same range gate of successive pulses. The transform will divide the frequency range, defined by one over the pulse repetition period, into equally spaced frequency bins. These bins would now define the frequency resolution of the radar. Any deviation from the center frequency is due to the Doppler shift caused by motion of the target with respect to the radar. The Doppler shift is a function of radial velocity only.

### **3. Major Recent Advances**

To fully understand radars of today several of the more important recent advances must be discussed. Of interest to this paper are the phased array and pulse compression techniques.

A phased array antenna system is an array of transmitting elements which work together to form the required beamshape. First consider a simple system with two radiating elements, separated by a specified distance. They will interact similar to that of the two slits in Young's double slit experiment. We see a far field intensity pattern defined by

$$I = I_1 + I_2 + 2(I_1 I_2)^{1/2} \cos(\delta) \quad (10)$$

with  $I$  = the total intensity;

$I_i$  = the intensity of element  $i$ ; and

$\delta$  = the phase factor.

With  $\theta$  being defined as the displacement from the center line divided by the range, the phase factor is then given by

$$\delta = (2\pi/\lambda) \sin(\theta) \quad (11)$$

By electronically altering the phase's of the signals sent to the radiating elements the constructive and destructive interference pattern is shifted off the center line. Through a direct extension of these theories it can be seen how this development allows for computer controlled beamshaping, steering and even multiple target tracking.

As stated earlier the range resolution of a radar is a function of the pulse width and this can be overly restrictive especially for high powered systems. To decrease this range there must exist a method to distinguish the front of one pulse from the end of the previous pulse. A simple method is to alter the frequency transmitted linearly as the pulse progresses. This method is called the chirped pulse. Another method is to phase encode the pulses. The phase of a sine wave is reversed based upon a specific sequence of phases. Shifting the phase increases the bandwidth of the sine wave. The main idea is that a phase encoded pulse has a short autocorrelation length. Thus on

reception when the pulse is correlated with itself the length is shortened and thus the resolution in range is smaller.

### III. PROBLEM

The data used for this thesis was from the installation in Hawaii. The NASA/JSC Transportable Radar System was deployed in a remote area near Hilo, Hawaii. Specifically, the radar consisted of several transmitter modules that could provided up to 250 kilowatts of peak pulse power at a two percent duty cycle, two coherent multi-channel receivers and several phased-array antenna systems.

The transmitter is a pulsed system which operated at 50 MHz. It was set to operate at a peak power of 160 KW with a duty cycle of one percent for this experiment. The pulse width was 50 microseconds and the pulse repetition period varied between 3000 and 5000 microseconds. The theoretical range resolution of the radar as defined by the pulse width is given by

$$R_{res} = \frac{c\tau}{2} = \frac{3 \times 10^8 \times 50 \times 10^{-6}}{2} = 7.5 \text{ km} \quad (12)$$

The theoretical unambiguous range of the radar is given by

$$R_u = \frac{c \times T}{2} = \frac{3 \times 10^8 \times 5 \times 10^{-3}}{2} = 750 \text{ Km} \quad (13)$$

The radar samples the data with a period of forty microseconds, which corresponds to six kilometres, which is slightly less than the range resolution of the radar but defines the range gate width. The waveforms were sampled and collected in forty-eight gates. This corresponds to 288 kilometres. The initial sample was at a range of 75 kilometres, and second time around echoes were also collected which extended the second initial range out to 825 kilometres.

The antenna was an electronically steerable phased array. A phased array is a series of elements which are excited individually with a controlled phase relationship which directs the beam. This steering and beamshaping is done by controlling

constructive and destructive interference patterns. The physical layout and beam pattern used for each pass are depicted in Figure 11.

The data made available for processing was from the first two passes over Hawaii, and covered 32 range gates with both in-phase and quadrature channels.

The first pass occurred from 177:14:52 to 177:14:59 GMT which list the day:hour:minute. The radar was pointed at an angle of 42 degrees off the ground until minute 56 when the beam was switched to a 54 degree angle. At 54 degrees the beam intersected the magnetic field line perpendicularly. During the first pass the meteor event rate was reported as relatively low with one to two events per minute and no natural E-region returns reported. The tethered system was predicted to pass through beam center at approximately 177:14:54:20 GMT (day:hour:minute:second), at a slant range of 980 kilometres.

Pass two occurred from 177:16:33 to 177:16:40 GMT. Data was only available for the first five minutes of pass two at which time the beam was directed at an angle of 58 degrees off the ground. The meteor event rate was slightly higher than pass one, up to about three to four events per minute. On this pass the tethered system crossed beam center at 177:16:35:35 at a slant range of 745 kilometres.

The data received is made up of background noise, unstable E-field echoes, meteor echoes and echoes caused by the Delta-PMG experiment. To correctly process the data, the types of echoes expected must be understood.

The background noise was found to have a fairly constant mean value and a small variance at each elevation of the radar. The autocorrelation function of several portions of echo free returns were tested and the results closely resembled that of the autocorrelation of white noise. The results were close enough to enable the background noise to be treated as white noise with no apparent loss of accuracy or validity.

#### **A. PROCESSING**

As stated earlier the meteor can produce several different types of returns. A very large meteor can, under proper conditions, produce a cloud of ions which have

similar properties to that of a plasma cloud. However; these types of returns are very infrequent and can be substantiated by other methods such as visual. The small meteor will produce a very sharp and well pronounced return which is easily distinguishable from a plasma cloud. Only the head of the meteor will reflect enough energy to be detected and will act very much like a hard target. The intermediate sized meteor will produce the largest problem as it will produce an ionized cloud, but the meteor head echo will be too small to make independent identification as a meteor difficult. The only other returns will be from the vehicle itself and unexpected targets that pass through the beam. All of these returns will be hard targets and show a definite and sharp signature.

As no obvious procedure or model for the expected signal was apparent several procedures were considered and rejected. All modeling techniques, tracking algorithms and correlation receivers were unsuccessful as no time or frequency characteristics completely separated all the various returns. The returns may contain a wide range of frequencies and may remain for varying lengths of time.

It has been established that the background noise can be taken as white noise with varying mean and variance at each of the range gates. The small meteors and various unexpected targets like aircraft or orbiting equipment that pass through the beam will be characterized by a straight forward return that is limited to one range gate and contain basically one frequency. The medium meteor may or may not contain a large distinct echo from the head of the meteor, it will produce an ionized cloud which will exhibit similar characteristics to that of a small plasma cloud and should transgress several range gates. The large meteor will have a very distinct head echo that transgresses many range gates, it should last for a substantial length of time and will produce a large ionized cloud in it's wake. The large meteor is easily confirmed by other sensors. The plasma cloud, which is the primary target of interest, will not have a constant hard return and the echo will resemble turbulence with scintillating intensity. The frequency contained in the return will be wide ranging and offset by a

Doppler shift if not exactly perpendicular to the radar beam. The frequency content of the echo is determined by the Short Time Fourier Transform (STFT) calculated using

$$\text{STFT}_x^\gamma(nT, kF) = \int_t x(t) \gamma^*(t-nT) e^{-j2\pi kFt} dt \quad (14)$$

with  $\gamma$  = rectangular window; and  
 $x$  = time series to analyzed.

The magnitude of the STFT was taken and plotted against time to form the spectrogram. The spectrogram by definition covers all frequencies between plus or minus one half the sampling frequency. As the range gates were sampled at the pulse repetition frequency of 200 Hz, the spectrogram analyzes the returns frequency components between -100 and 100 Hz. The Doppler shift imparted on a return relates directly to the targets radial velocity with respect to the radar. If the angle of incidence of the target with respect to the axis of the radar beam is known the target's velocity can be calculated using

$$V_r = f_d c / (2f_t \cos(\theta)) \quad (15)$$

with  $f_d$  = Doppler shift (Hz);  
 $f_t$  = transmitted frequency (Hz);  
 $c$  = speed of light (m/sec);  
 $V_r$  = radial velocity (m/s); and  
 $\theta$  = angle of incidence of target (rad).

A positive Doppler shift indicates the target is closing on the radar, while a negative Doppler indicates the target is moving away.

By determining which returns exhibit the characteristics of plasma echoes we can quickly eliminate those which are definitely not the plasma-perturbations caused

by the satellite's movement through the ionosphere. To determine which returns exhibit the proper characteristics we note that a plasma cloud is an area of highly ionized particles. As discussed earlier in the paper, the electrons are the main reflecting element. The cloud has areas of varying electron density which are in constant motion and produce a return of scintillating intensity. The plasma cloud can also be described by turbulence theory. Although the intensity fluctuations appear random they are correlated when the power spectral density plot is observed. As the cloud does not have a constant mean it can not be treated as stationary and conventional statistics are of limited use. Instead the more robust structure function formulations are needed. A structure function is the mean square difference between two intensity measurements at two different locations in space. The structure function has the form

$$D_x(\underline{r}_1, \underline{r}_2) = \langle [x(\underline{r}_2) - x(\underline{r}_1)]^2 \rangle \quad (16)$$

with  $x(\underline{r}) =$  intensity at position described by  $\underline{r}$ ; and  
 $\langle \rangle =$  time averaging.

The structure function is similar to a variance measurement but removes the mean value and slow changes in the mean. Structure functions are also tensors in general and depend on the vectors depicting the measurement locations. Frequently it is possible to assume local homogeneity and isotropy in limited volumes of space the structure function becomes proportional to the scalar separation distance between measurements. With these assumptions the power spectrum becomes proportional to the first difference between measurements raised to some power

$$(17) \quad D_x[|\underline{r}_2 - \underline{r}_1|] = C^2 r^m$$

with  $C =$  some constant;  
 $r =$  distance between measurements; and  
 $m =$  some power to be determined.

Kolmogorov turbulence defining flow with a Reynolds number greater than 100,000 have often been shown to have a dependence of the first difference raised to the two-thirds power. This dependence is valid over separations ranging from millimetres to meters. The connection between the structure function and the autocorrelation function can be seen by expanding equation (16). When expanded it takes on the form

$$D_x(r_1, r_2) = 2 \langle x^2 \rangle - 2 \langle x_2 x_1 \rangle \quad (18)$$

Where the first term relates to the variance and the second term shows the direct connection to the autocorrelation function. As well, the power spectral density is the Fourier Transform of the autocorrelation function. Therefore; a plasma cloud should be identifiable from an autocorrelation plot and power spectral density plot of its returns. [Tennekes and Lumley, 1974]

The biased autocorrelation function is estimated using

$$R_x[l] = (1/N) \sum_{n=0}^{N-l-1} x[n+l] x^*[n] \quad (19)$$

with  $l =$  the time lag from 0 to  $N$ ;  
 $x =$  the data sequence from a set range gate; and  
 $N =$  the number of data points used.

The autocorrelation function of a solid target will display a sharp main lobe and then will drop off quickly and in a regular manner as the time lag  $l$  is increased. For a scintillating target such as plasma, the autocorrelation function will show a thinner main correlation lobe but will display side lobes at larger time lags.

## IV. OBSERVATIONS

The procedure defined in the previous section was used to analyze the data supplied.

### A. PASS ONE

During the first pass thirty three range gates contained echoes with sufficient power to be declared a target. Target detection was based on power, with the in-phase and quadrature channel outputs squared and added. The detector threshold was determined by the operator visually. The number of returns prohibit attaching all returns, so only those deemed necessary or interesting will be included in the thesis.

Figure 12 shows the plot of range gate ten for the 58<sup>th</sup> minute that was used for initial declaration of a target. The in-phase and quadrature channel outputs were squared and summed and then plotted versus time. In this figure we see that the target is above the threshold for a very short duration of time.

Figure 13 shows the declared target from Figure 12 but this time it displays the first sixteen range gates versus a reduced time scale as well as it's spectrogram. The range gates plotted versus time show a target with a duration of approximately 0.1 to 0.2 seconds. The return is in only one range gate and very strong. The spectrogram shows a strong frequency center with all frequencies present but their contribution drops off as they extend out from the center frequency. The slightly elongated time span is due to the fifty percent overlap processing used. The center frequency varied with time as if the target was changing aspect with respect to the radar or speed.

Figure 14 shows the same detection sequence used earlier but for range gate six during the 58<sup>th</sup> minute. The signal is located at approximately thirty one seconds and exceeds the threshold for almost two seconds. The signal power peaks at the start of the return and declines as time progresses.

Figure 15 displays the declared target from Figure 14 but this time it shows the first sixteen range gates and the returns spectrogram plotted versus a reduced time

scale. By plotting all sixteen range gates versus time we see that this target's return is spread over three range gates, with a duration of approximately one second and is scintillating in intensity. The spectrogram shows a similar scintillating nature with a poorly defined center frequency and a large spread of frequencies present. The wide spread of frequencies present at the onset of the return seem to dissipate to the point where only the center frequency is present.

The echoes with features to those presented in Figures 12 and 13 are deemed to be either a meteor with a small trail or an extraneous hard target. Echoes displaying the characteristics found in Figures 14 and 15 are deemed to be a large meteor trail or plasma. The large meteor required to produce these characteristics would be easily verified by other methods. Only when the echo's spectrogram and is viewed in conjunction with several range gates plotted against time can these determinations be made. This procedure is computationally burdensome, but as discussed earlier a single plot of the autocorrelation function can quickly eliminate the majority of echoes not caused by plasma. This can be easily seen by viewing the autocorrelation functions of the previously discussed echoes. Figure 16 shows the wide main lobe and low correlation at large time lags for the target from range gate ten, while the bottom plot shows the sharp main lobe and repetitive side lobes at large time lags of the target from range gate six. Unfortunately, finer discrimination still requires using the spectrogram and the range gate plots.

Thirty three declared targets from pass one were analyzed; selected returns are presented.

During minute 52 of the first pass there were only three returns. Figure 17 shows the spectrogram and autocorrelation function of the return in the sixteenth range gate. This target was a very weak return but is noticeable for the long and scintillating nature of the echo's spectrogram. It displays a positive Doppler shift and lasts from twenty to about twenty five seconds. The autocorrelation function shows a very sharp peak and displays correlation at large time lags. The other return in this minute is

mainly located in the seventeenth range gate with a small portion of the energy in the eighteenth range gate. Figure 18 shows the spectrogram and autocorrelation function of the return from the seventeenth range gate. In this figure the return exhibits a negative Doppler shift which corresponds to a negative target velocity component in the radial direction. The return is present from about eighteen and three quarters to twenty one seconds. The autocorrelation function of this return shows a very distinctive correlation pattern at large time lags. The return from range gate sixteen is too weak to enable a plot of several range gates against time to reveal any information. These two returns are classified as plasma.

The fifty third minute has the most range gates with sufficient energy to have a target declared. The majority of the returns during this minute occur between twenty two to twenty eight seconds. Figure 19 shows the first sixteen range gates plotted versus time to show the returns with relationship to each other. In this figure we see several sharp short duration echoes and one scintillating longer duration return. The majority of these returns transgress more than one range gate. Figure 20 shows the autocorrelation function and the spectrogram of the echo from range gate five at approximately 24.8 seconds. This figure shows a spectrogram localized in time with a frequency center Doppler shifted by twenty Hz. The autocorrelation function shows a wide main lobe with very little correlation at larger time lags. Figure 21 contains the spectrogram and autocorrelation function of the return from range gate six centered at approximately twenty four seconds. The spectrogram shows what looks like two localized returns with a scintillating return connecting them. The autocorrelation function seems to reflect this combination of attributes. The main lobe is very narrow and the correlation function drops off quickly to near zero but the larger time lags show definite correlation. Figure 22 shows the spectrogram and autocorrelation function of the return from range gate nine at approximately twenty three seconds. In this figure we see a scintillating pattern in the spectrogram that shows a negative

Doppler shift with a very short duration of about one half of a second. The autocorrelation function displays a very narrow main lobe and high sidelobes; however, they decay very quickly.

During minutes fifty four, fifty five, fifty six and fifty seven all the returns except one were short in duration and displayed low correlation at the larger time lags. The one return not of this form was detected in range gate twenty two at approximately one second. Figure 23 shows the spectrogram and autocorrelation function of this return. In the figure we see that the spectrum contains a very localized frequency component which is Doppler shifted by negative twenty Hz. The signal lasts for almost two seconds and with two short drops in intensity during the return. The autocorrelation function shows a wide main lobe with dips matching the drops in intensity of the signal.

The fifty eighth minute contained two large returns. Figure 24 shows the sixteen range gates versus time. This figure shows the two large returns and their orientation to each other. The return starting at approximately thirty two seconds is larger than the return starting at approximately 26.5 seconds and is at a larger slant range. Both returns are scintillating in nature and transgress more than one range gate. Figures 25 and 26 show the spectrogram and autocorrelation function for these returns using the range gate containing the most power for each return. Figure 25 is the spectrogram and autocorrelation function for the return from range gate three at approximately twenty seven seconds. In this figure the spectrogram of the return shows a scintillating return with no Doppler shift. The autocorrelation function displays a very repetitive structure and a definite correlation at large time lags. Figure 26 displays the spectrogram and autocorrelation function of the return from range gate six located at approximately thirty two seconds. The figure shows very similar characteristics as those observed in Figure 25, but with a larger intensity. These two returns are deemed to be from plasma.

## **B. PASS TWO**

The majority of echoes from pass number two were short in duration and had a localized frequency spectrum which indicated that they were returns from meteors.

Figure 27 shows the spectrogram and autocorrelation function of the echo from range gate four, during minute thirty four at approximately 46 seconds. The form displayed in this figure also represents the return from range gate five at the same time. The spectrogram shows a scintillating return with a Doppler shift of approximately twenty five Hz. The autocorrelation function has a narrow main lobe with correlation at larger time lags.

Figure 28 contains the spectrogram and autocorrelation function of the echo from range gate nineteen, during minute thirty seven at approximately thirty seven seconds. These plots accurately reflect those for the return from range gate eighteen at the same time. The spectrogram shows a very strong quasi-static, direct current component that lasts for almost two seconds and a repetitive structure that covers the entire frequency band tested.

## V. POST ANALYSIS

The first two passes over the radar site in Hawaii were analyzed. This data was composed of thirty two range gates sampled 200 times every second for twelve minutes. Every single one of the over five million samples were analyzed at least once, with those deemed to be corresponding to a valid return being analyzed completely. This exhaustive analysis resulted in several observations.

Initially the returns can be separated by the use of the autocorrelation function. The majority of the meteor echoes will display an autocorrelation function that has a wide main lobe and very little correlation at larger time lags. A plasma cloud will exhibit a spectrogram displaying scintillating intensity and an autocorrelation function which has a sharp narrow main lobe with correlation at larger time lags.

Unfortunately, not all returns fall exactly into these two cases and must be reviewed more closely, and not all returns displaying the characteristics of plasma will be caused by the passage of the tethered system through the ionosphere. Plasma is present in the ionosphere and if unstable may produce a return, or a large meteor ionizing the ionosphere produces a target with characteristics similar to that of plasma.

The presence and direction of motion and the echo's orientation with respect to other targets will provide a method of separating spurious returns or meteors from the plasma of interest for this thesis. All plasma clouds will have motion, either self imposed or by ionospheric winds. The target of interest in this thesis is a plasma cloud that travels along the Earth's magnetic field line in one direction and then crosses to another field line before travelling in the opposite direction to complete the circuit.

All returns not specifically discussed in this section have been classified as a hard target or meteor. Figures 17, 18, 21, 22, 23, 25 and 26 display characteristics inconsistent with a meteor.

Figures 17 and 18 show the two returns from minute fifty two. During this minute the antenna beam was not perpendicular to the Earth's magnetic field lines and

thus anything travelling along the field lines will display a positive or negative Doppler shift depending on the direction of travel. Both echoes display the properties of plasma and are separated by a range gate and almost two seconds. The later return is much weaker in intensity but is at a shorter slant range. Figure 17 shows an echo with a positive Doppler shift and Figure 18 shows an echo with a negative Doppler shift. For these reasons these echoes are deemed to be from the same target and caused by the Delta-PMG experiment.

Figure 22 shows the large scintillating return from range gate nine during minute fifty three. This figure show that this echo displays all the attributes of plasma; however, the echo has no matching return and the correlation decays very quickly. This implies that this echo was caused by some other phenomenon.

Figures 21 and 23 show two non-standard returns. Figure 21 displays what appears to be two solid targets connected by a plasma cloud. Although unconfirmed by vehicle trajectory this target should be investigated as being caused by the vehicle. Figure 23 is definitely a hard target but is peculiar by its duration. This target is interesting but definitely not caused by the passage of the tethered system through the ionosphere.

Figure 24 displays two echoes received during minute fifty eight with Figures 25 and 26 displaying these two echoes individually. During minute fifty eight the antenna beam was pointed perpendicular to the magnetic field lines which means that any motion along these magnetic field lines will not produce a Doppler frequency shift. Neither target displays a Doppler frequency shift and it is apparent that these two echoes are plasma. As well their location and time of detection with respect to each other imply that the echoes are in fact from the same plasma cloud. These facts lead to the conjecture that these returns are from a plasma cloud created by the space tether.

The echo from pass number two shown in Figure 26 is definitely not from a plasma cloud. It is however very similar to that shown in Figure 21 from pass number

one. The fact that this echo format is found only once per pass but in each pass could indicate a more in depth analysis of its origin is in order.

Figure 25 displays the characteristics of a plasma target; however, the beam during pass number two was nearly perpendicular to the Earth's magnetic field line and the amount of Doppler shift exhibited by this target make it very unlikely that it was caused by a plasma cloud travelling along the field line.

Table one gives a comprehensive review of the targets analyzed from pass one. Each row of the table represents the return from a single target and may appear in several range gates. As well, each target has been declared either a hard or soft target. A soft return is from a suspected plasma target, where as the hard return is from any target other than plasma. The Doppler shift listed in the table is the Doppler shift associated with the echo's center in Hz. This was calculated by summing across each frequency bin in the Spectrogram to find the maximum magnitude. For each return the associated figure number, if any, is listed in the final column.

| TIME<br>(MIN:SEC) | RANGE<br>GATES | DURATION<br>(SEC) | HARD/SOFT<br>RETURN | DOPPLER<br>SHIFT | FIGURE<br>NUMBER |
|-------------------|----------------|-------------------|---------------------|------------------|------------------|
| 52:21             | 16             | 3 - 4             | SOFT                | 28 Hz            | # 17             |
| 52:19             | 17,18          | 3.0               | SOFT                | -15 Hz           | # 18             |
| 53:23             | 8,9,10         | 0.5               | SOFT                | -20 Hz           | # 22             |
| 53:26             | 1,2            | 0.25              | HARD                | NIL              |                  |
| 53:24             | 4,5            | 0.25              | HARD                | 15 Hz            | # 20             |
| 53:23             | 6              | 1.0               | SOFT                | 20 Hz            | # 21             |
| 54:22             | 8              | 0.1               | HARD                | NIL              |                  |
| 55:46             | 5              | 0.1               | HARD                | NIL              |                  |
| 55:17             | 7              | 0.1               | HARD                | NIL              |                  |
| 55:35             | 14             | 0.1               | HARD                | -12 Hz           |                  |
| 56:33             | 2              | 0.25              | HARD                | NIL              |                  |
| 56:15             | 13             | 0.25              | HARD                | NIL              |                  |
| 56:01             | 22             | 2.0               | HARD                | -20 Hz           | # 23             |
| 57:10             | 2              | 0.25              | HARD                | 18 Hz            |                  |
| 57:24             | 3              | 0.25              | HARD                | 15 Hz            |                  |
| 58:26             | 3,4            | 1.0               | SOFT                | NIL              | # 25             |
| 58:32             | 5,6,7          | 1.5               | SOFT                | -2 Hz            | # 26             |
| 58:54             | 10,11          | 0.25              | HARD                | 5 Hz             |                  |

Table 1. Review of Targets Detected From Pass One

## VI. CONCLUSIONS

NASA conducted the Delta-PMG tethered satellite mission to verify basic characteristics of electrodynamic tether behaviour. A major element was the ability of a hollow cathode plasma source to couple electric current from each end of the tether to the ambient ionospheric plasma. A major question was how these currents travel into and through the plasma. It is thought that either plasma from the hollow cathodes, or a disturbance caused by the passage of the tether, propagates along the magnetic field line, away from the tether. The object of this thesis was to process the data obtained from the radar station in Hawaii to study disturbances in the Earth's ionosphere caused by the tether. The data processing was complicated by the presence of numerous other returns, primarily from meteors.

During the first pass over Hawaii two separate sets of returns were detected that were deemed to be induced plasma travelling along the Earth's magnetic field lines. These returns were deemed to be non-meteor returns based on their frequency content, Doppler shift and autocorrelation function. The disturbances detected in each set were interpreted to be propagating down one field line and back up another. The returns were observed prior to and after the passing of the vehicle through the antenna beam. The return following the passage of the tether occurred during minute fifty eight. This occurrence coincided with expectations established by previous observations. Disturbances detected prior to the tether passage, during minute fifty two, do not coincide with previous expectations. The actual passing of the vehicle was not detected. The second pass over Hawaii did not noticeably extend the results obtained from pass number one. The fact that no plausible returns were found while processing pass number two could be due to changing atmospheric conditions, the position and direction of the antenna beam or even the digitizing process.

The radar data indicates that the tether passage disturbs the ionosphere in such a way as to trigger a disturbance which propagates along magnetic field lines, perhaps due to plasma from the hollow cathodes. This may reflect the current coupling process

which controls the electrodynamic tether behaviour. It is recommended that all remaining data from this experiment be analyzed using the method put forward in this thesis to provide a more substantial base from which to study the phenomenon produced by the interaction between a long conducting tether and the Earth's magnetic field lines. The data concerning the disturbance in the ionosphere caused by the passage of the tether found during minute 58 and supplied orbital data for the tethered satellite system was used to extract velocity information for the travelling plasma disturbance.[Olson, 1994]

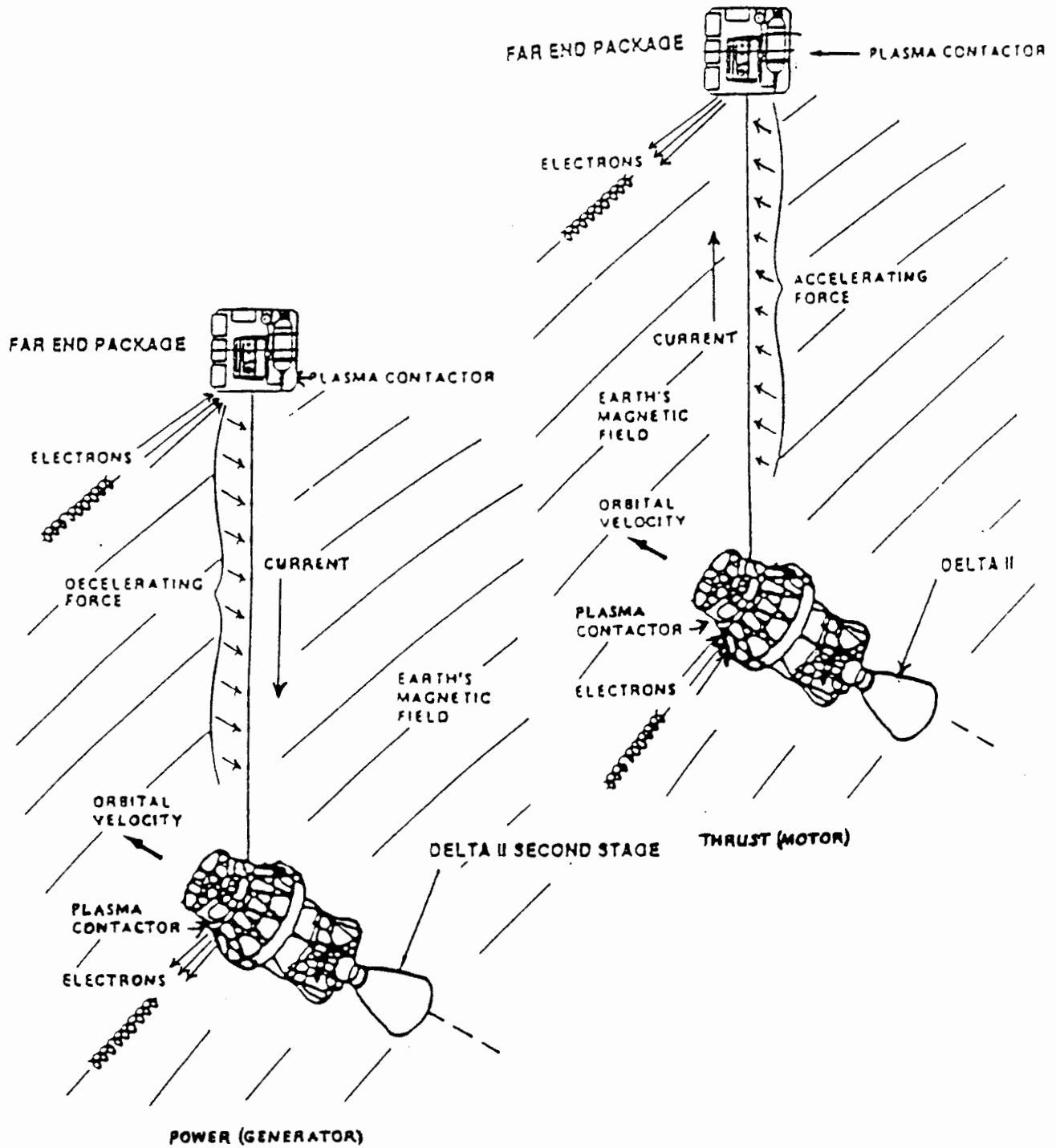


Figure 1. Electrodynamic Tether Principles [Fig 1 from Jost, 1994]

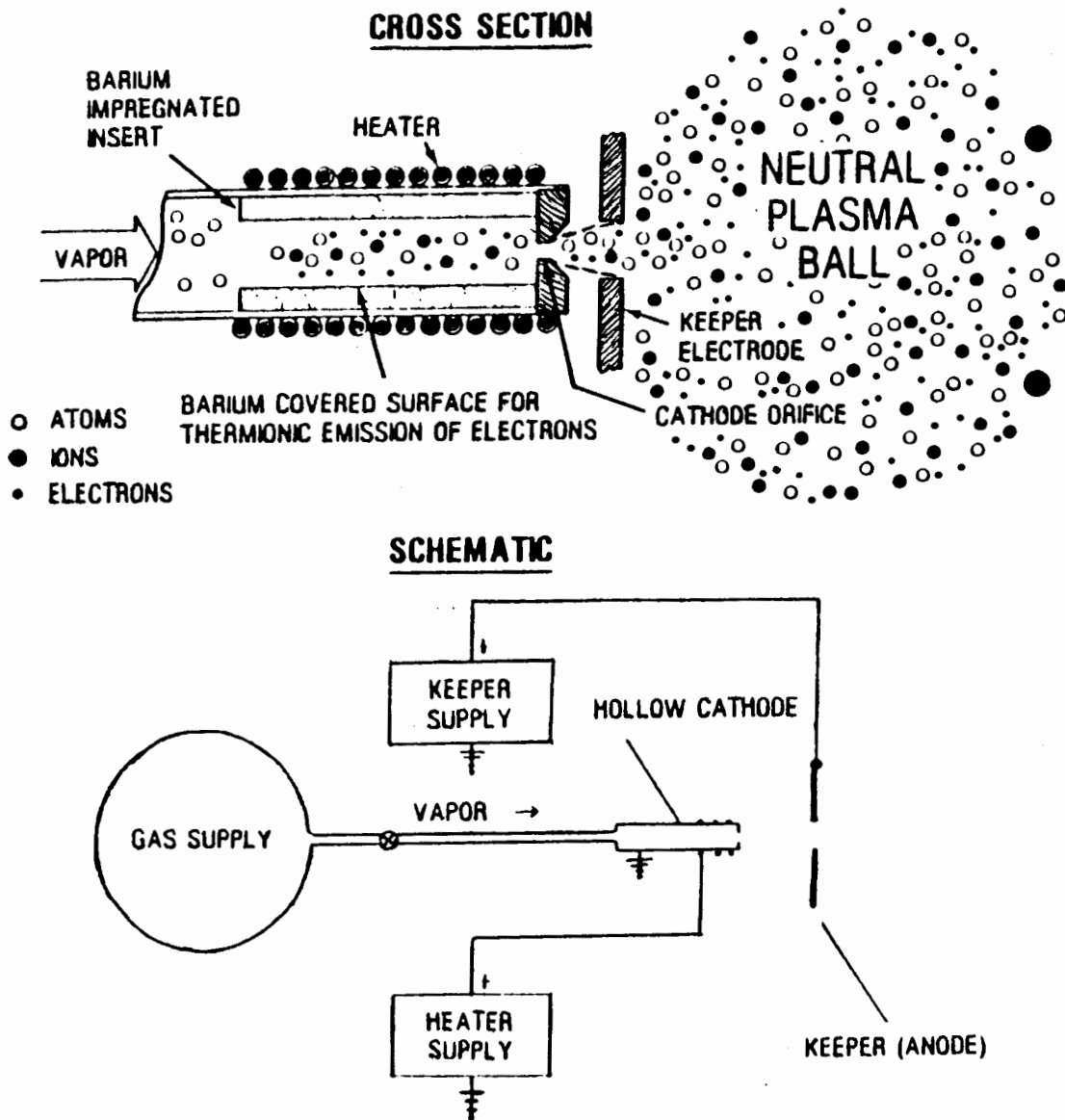


Figure 2. PMG Hollow Cathode Assembly [Fig 2 from Jost, 1994]

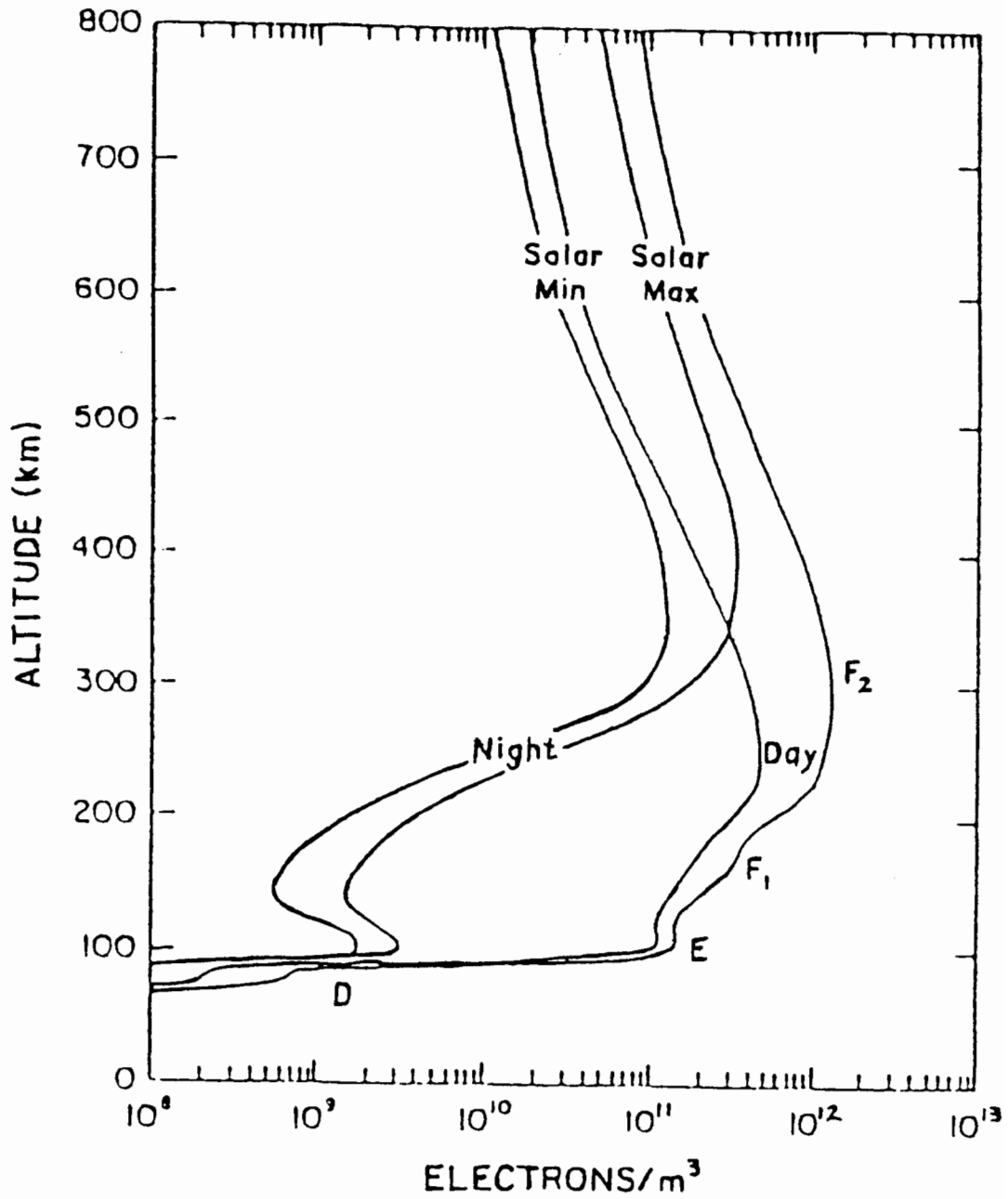


Figure 3. Typical Ionospheric Electron Density Profiles

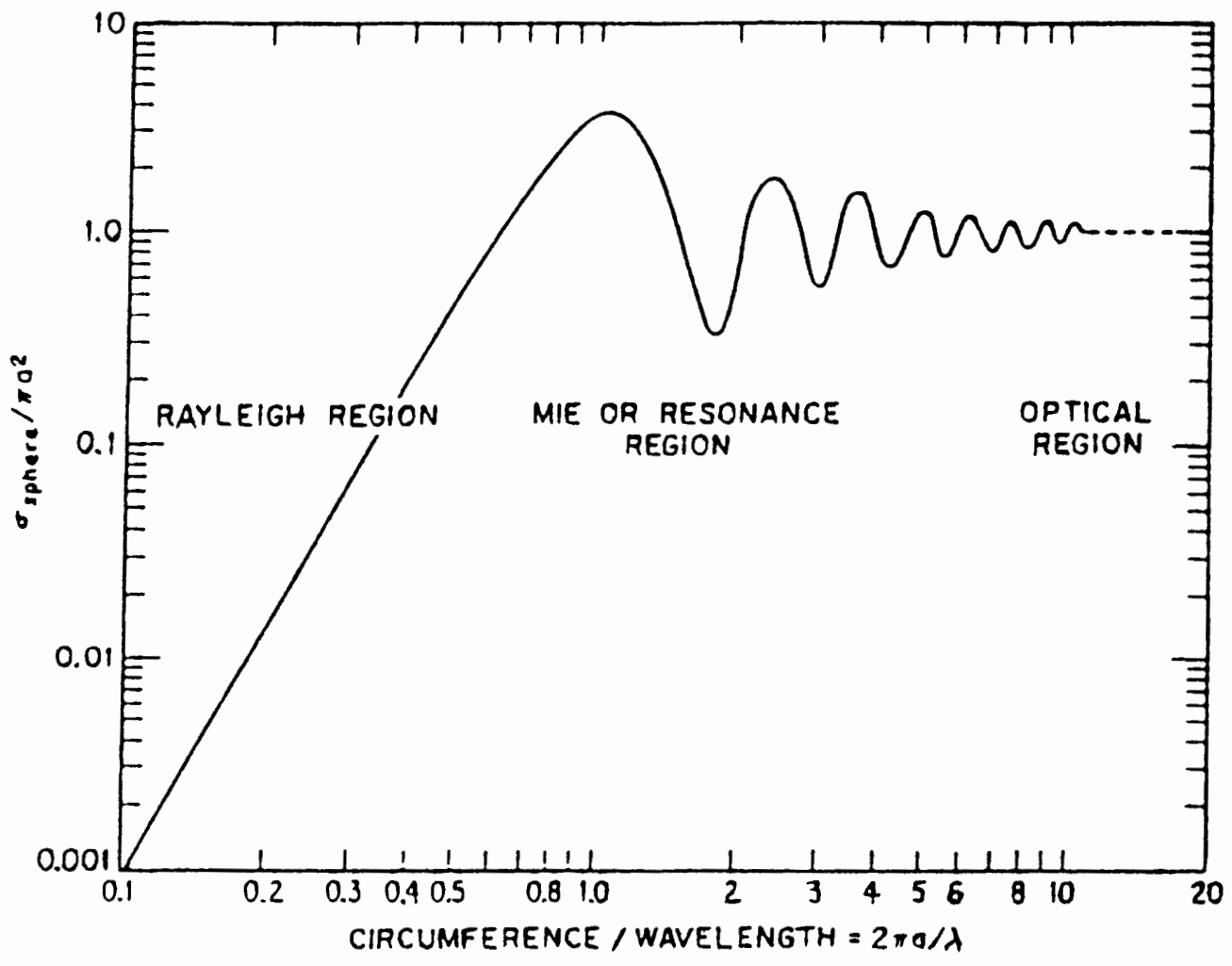


Figure 4. Radar Cross Section vs Wavelength [Skolnik, 1980]

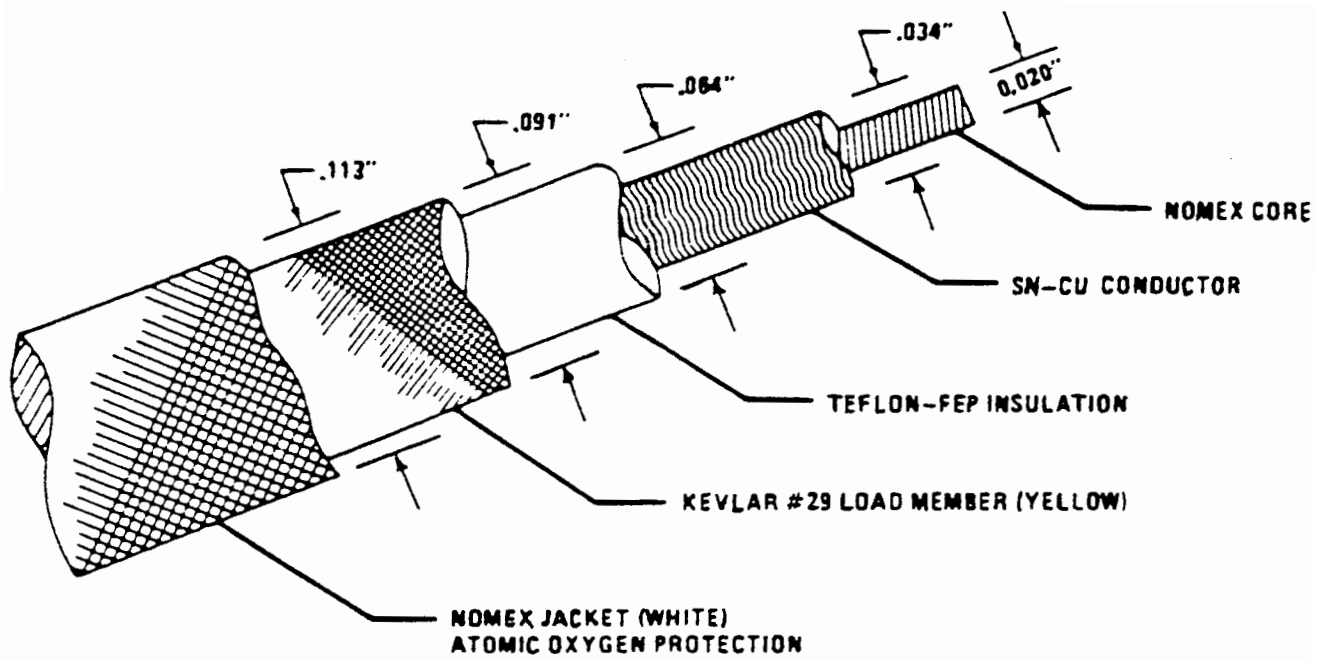


Figure 5. TSS-1 Conducting Tether [NASA, 1986]

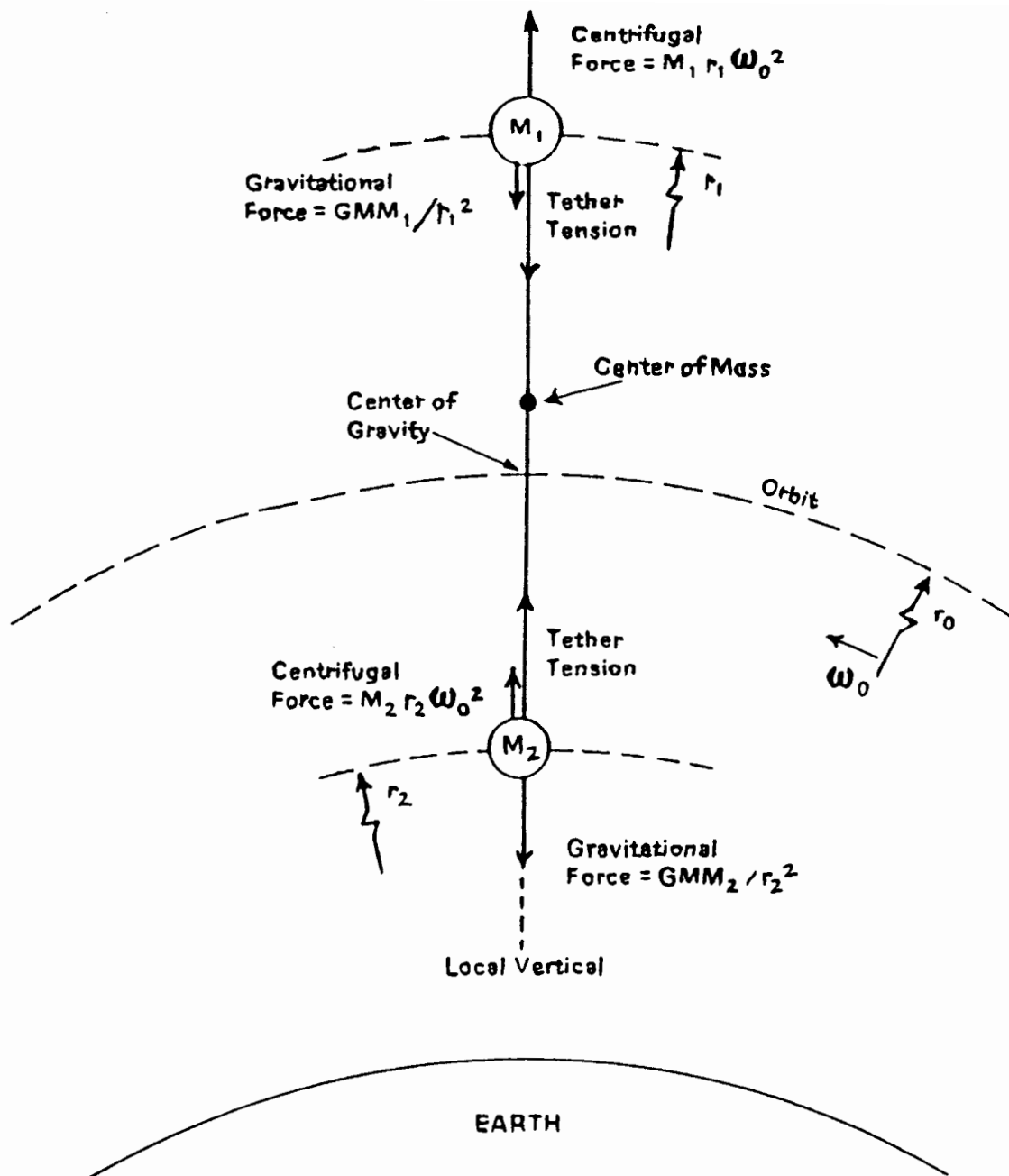


Figure 6. Forces on Tether System [NASA, 1986]

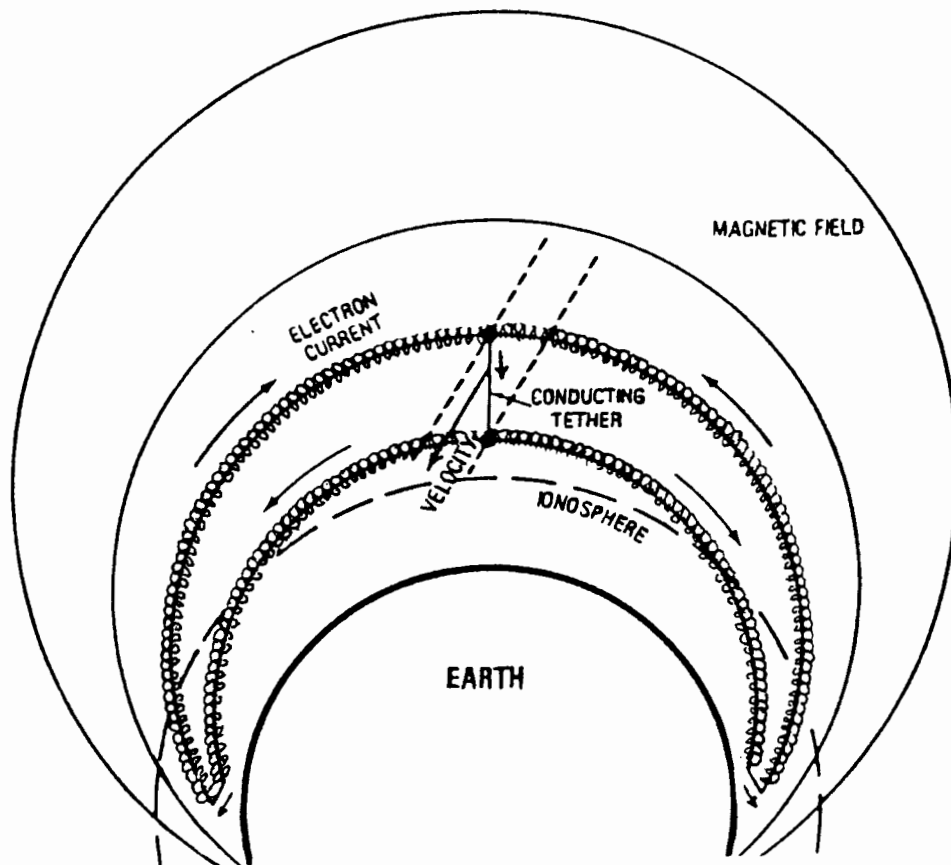


Figure 7. Phantom Current Loop [Fig. 5 from Jost, 1994]

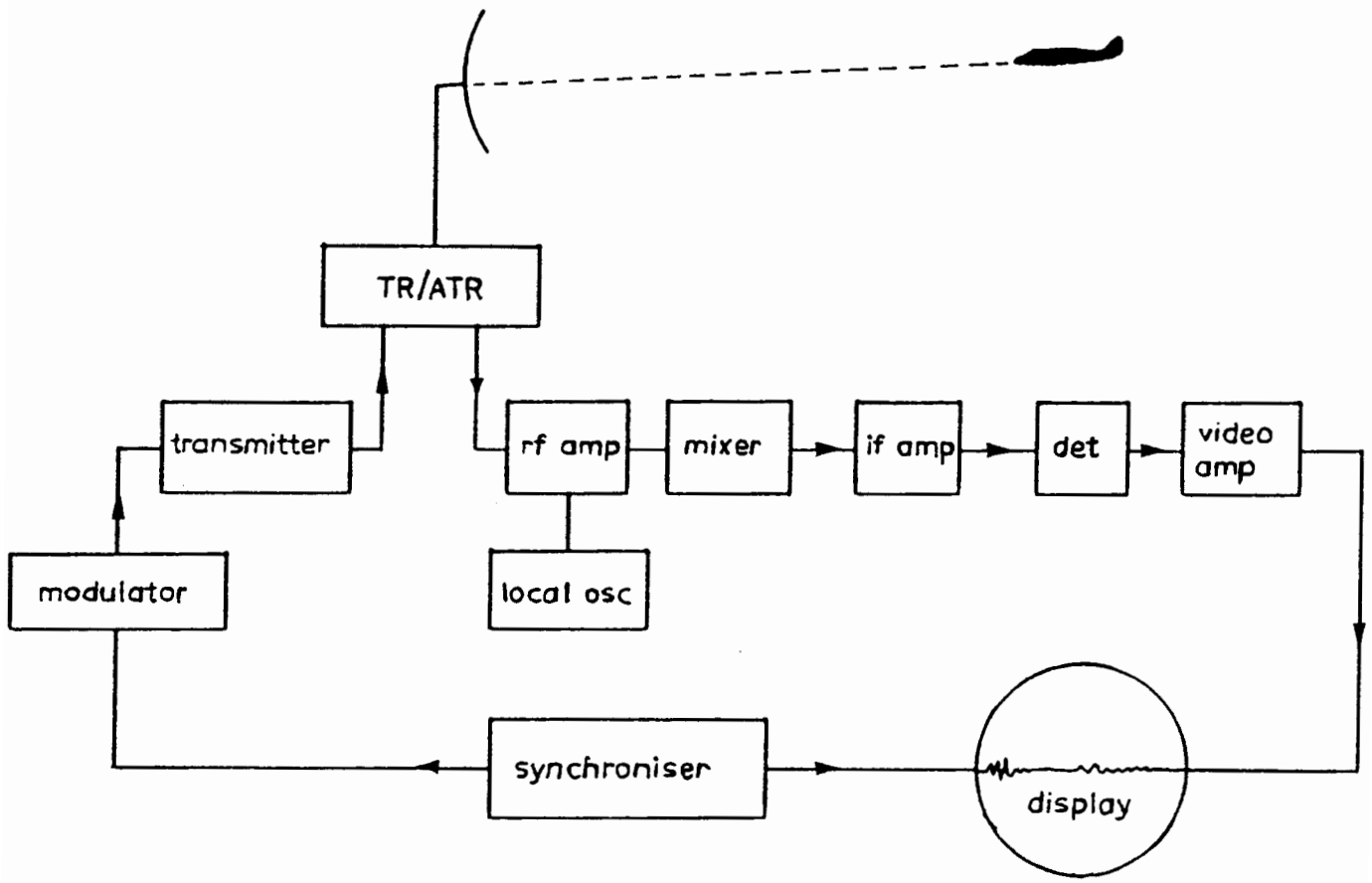


Figure 8. Basic Block Diagram [Fig. 2.6 from Swords, 1986]

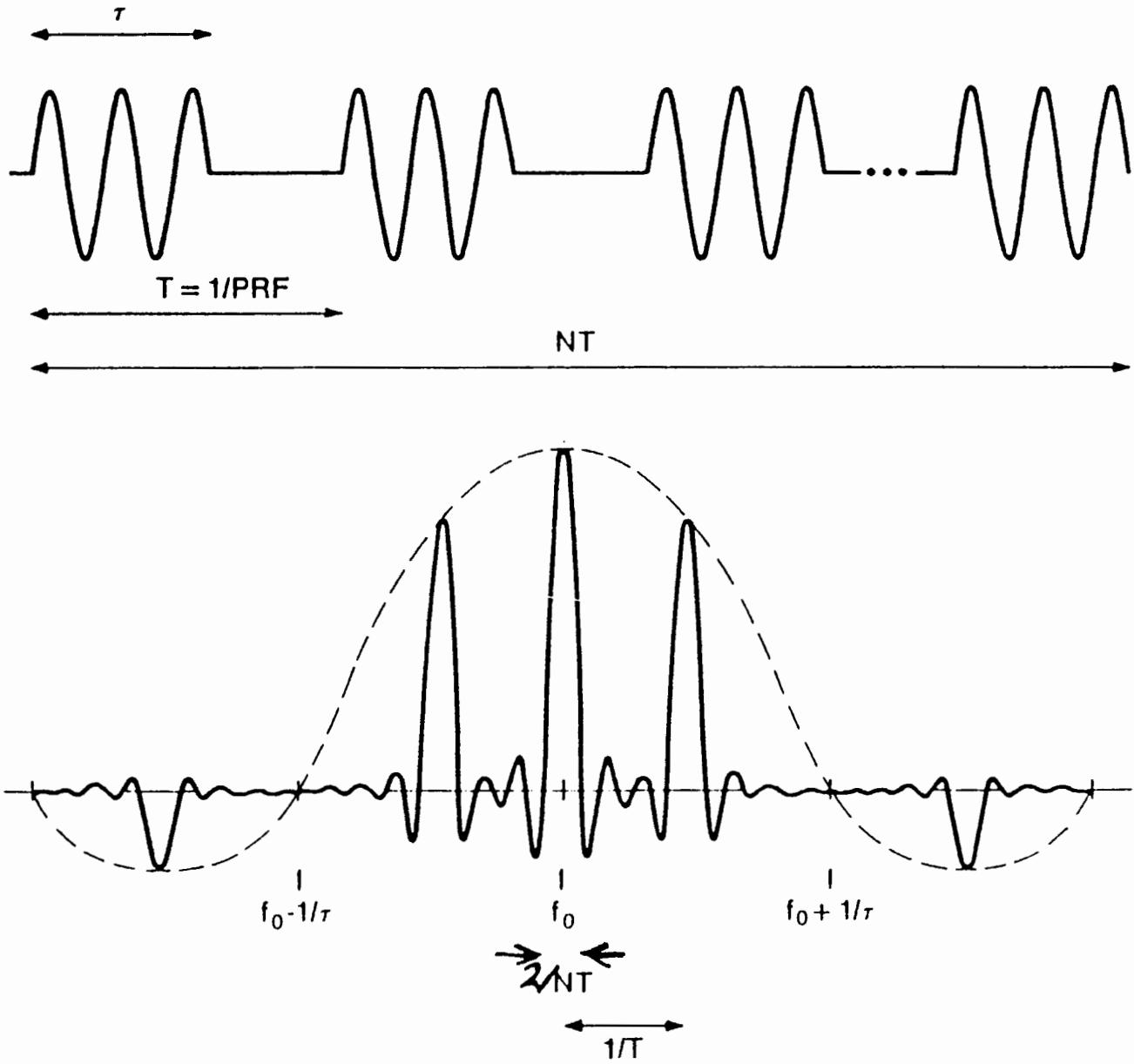


Figure 9. Digital Pulse Train and Fourier Transform

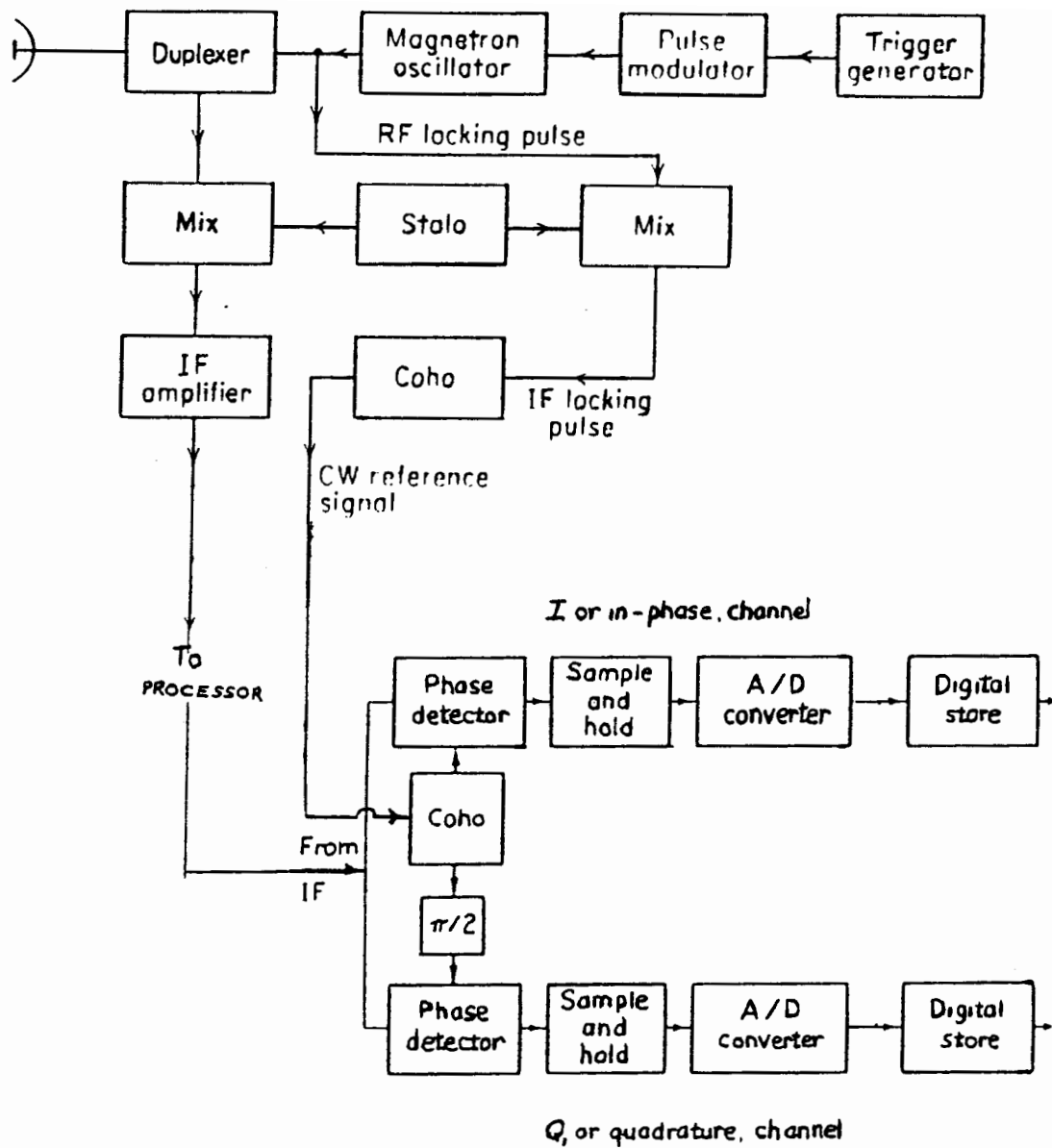
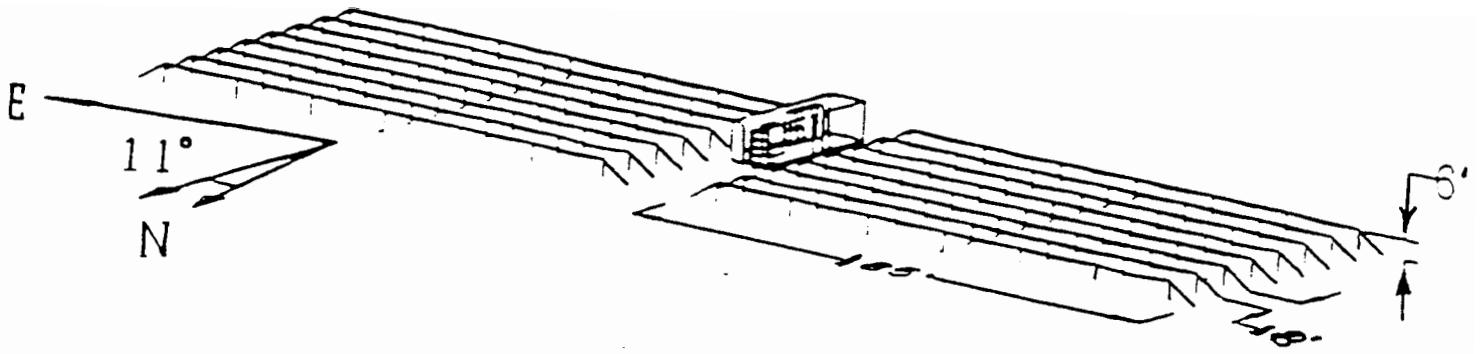


Figure 10. General MTI Receiver [Skolnik, 1980]



a. Physical dimensions and orientation

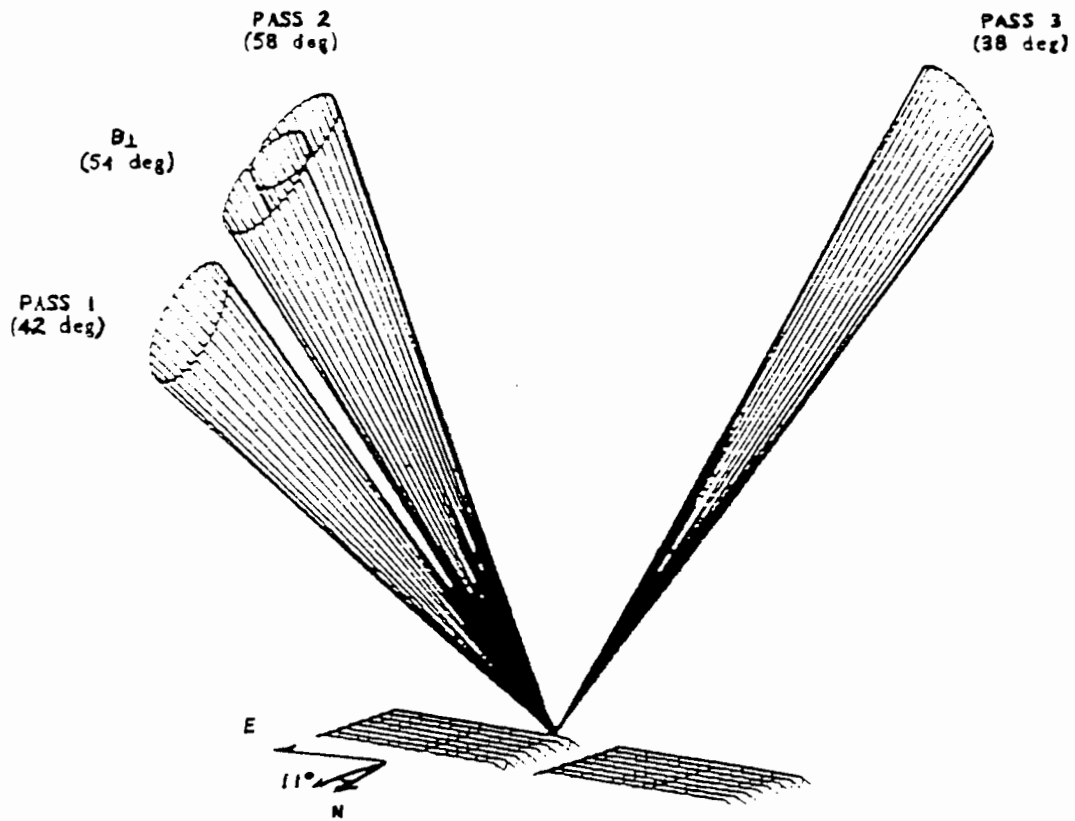


Figure 11. Phased Array Antenna System [Jost, 1994]

Power Detector ( $I^2+Q^2$ ) Output

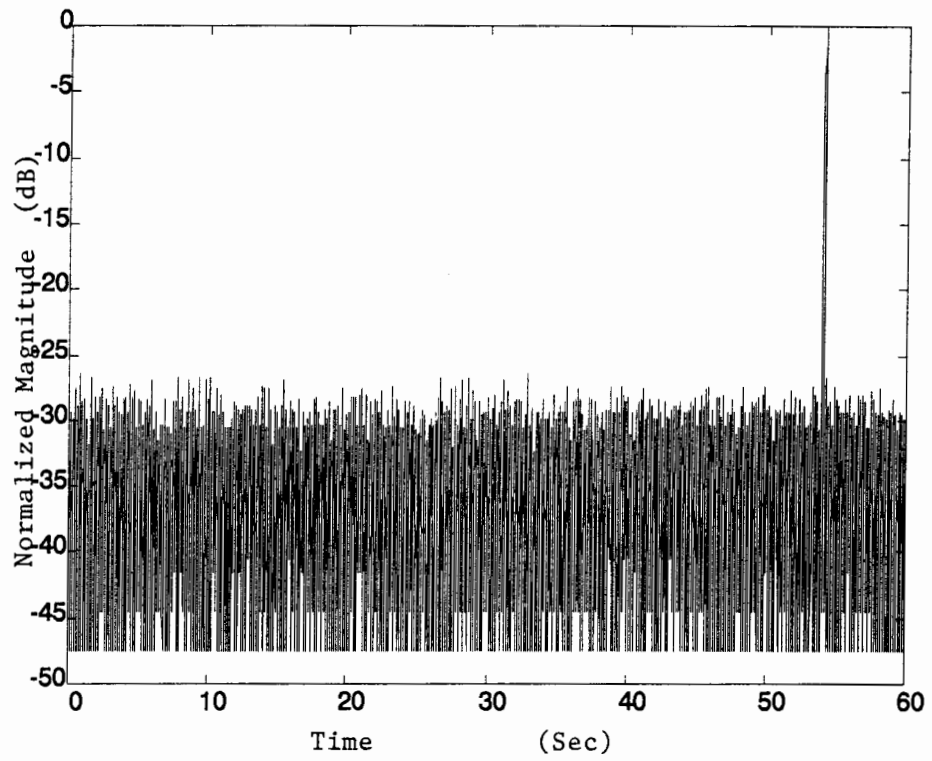


Figure 12. Meteor - Power Detector Output

PMG Pass 1: Time 14 58

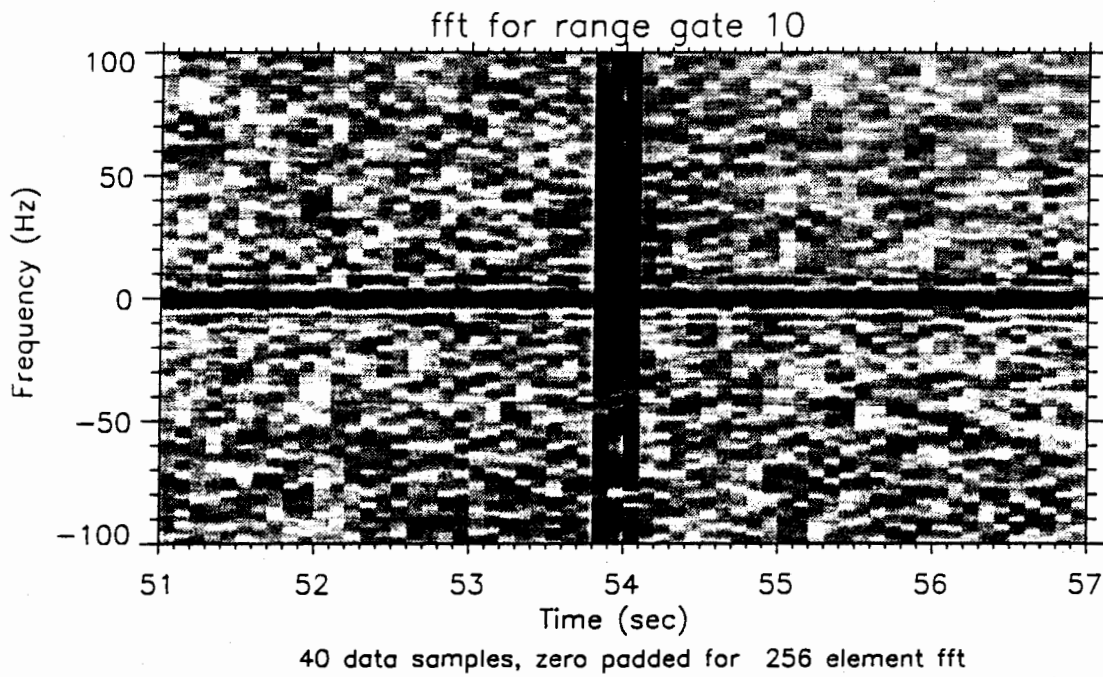
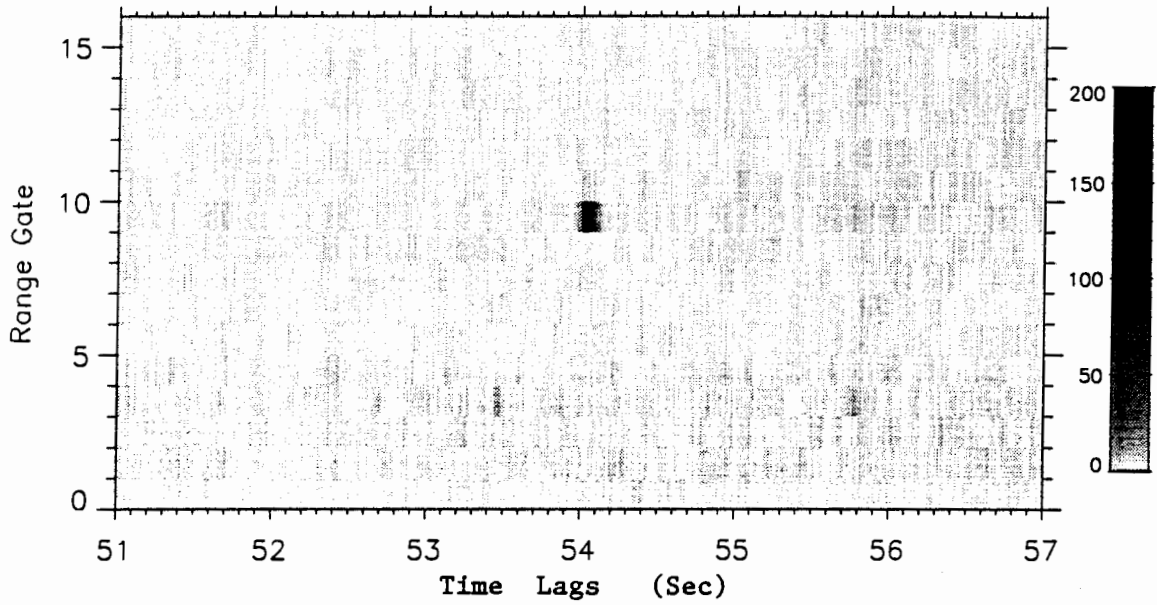


Figure 13. Meteor - Range Gates vs. Time and Spectrogram

Power Detector ( $I^2+Q^2$ ) Output

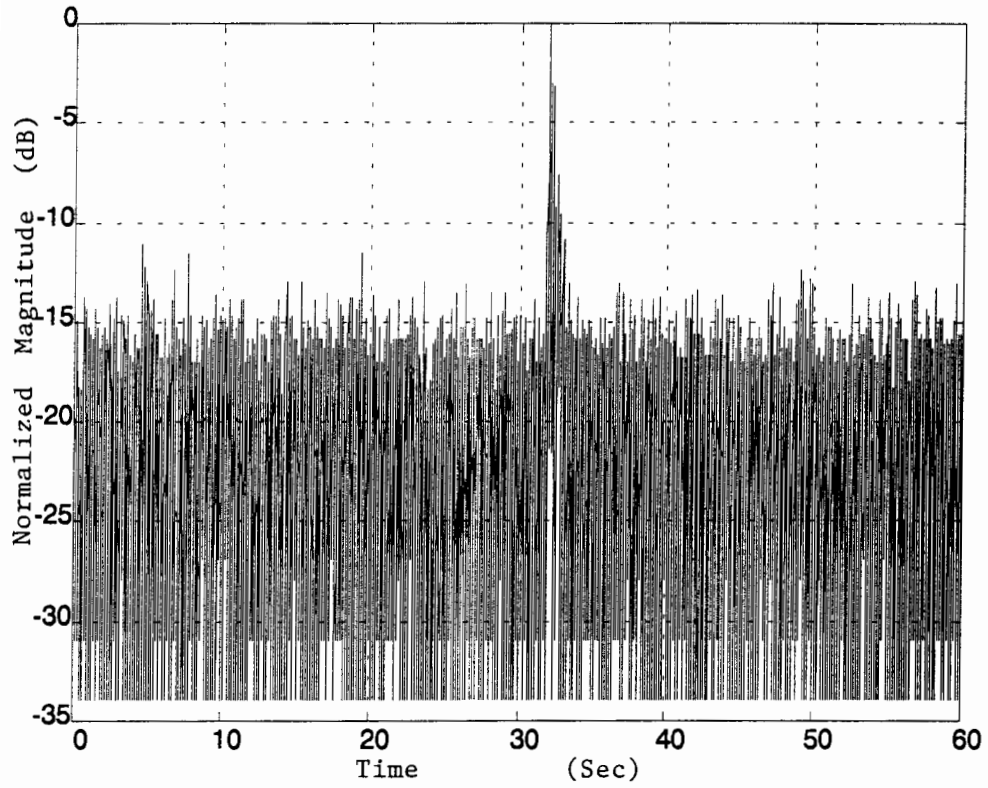


Figure 14. Plasma - Power Detector Output

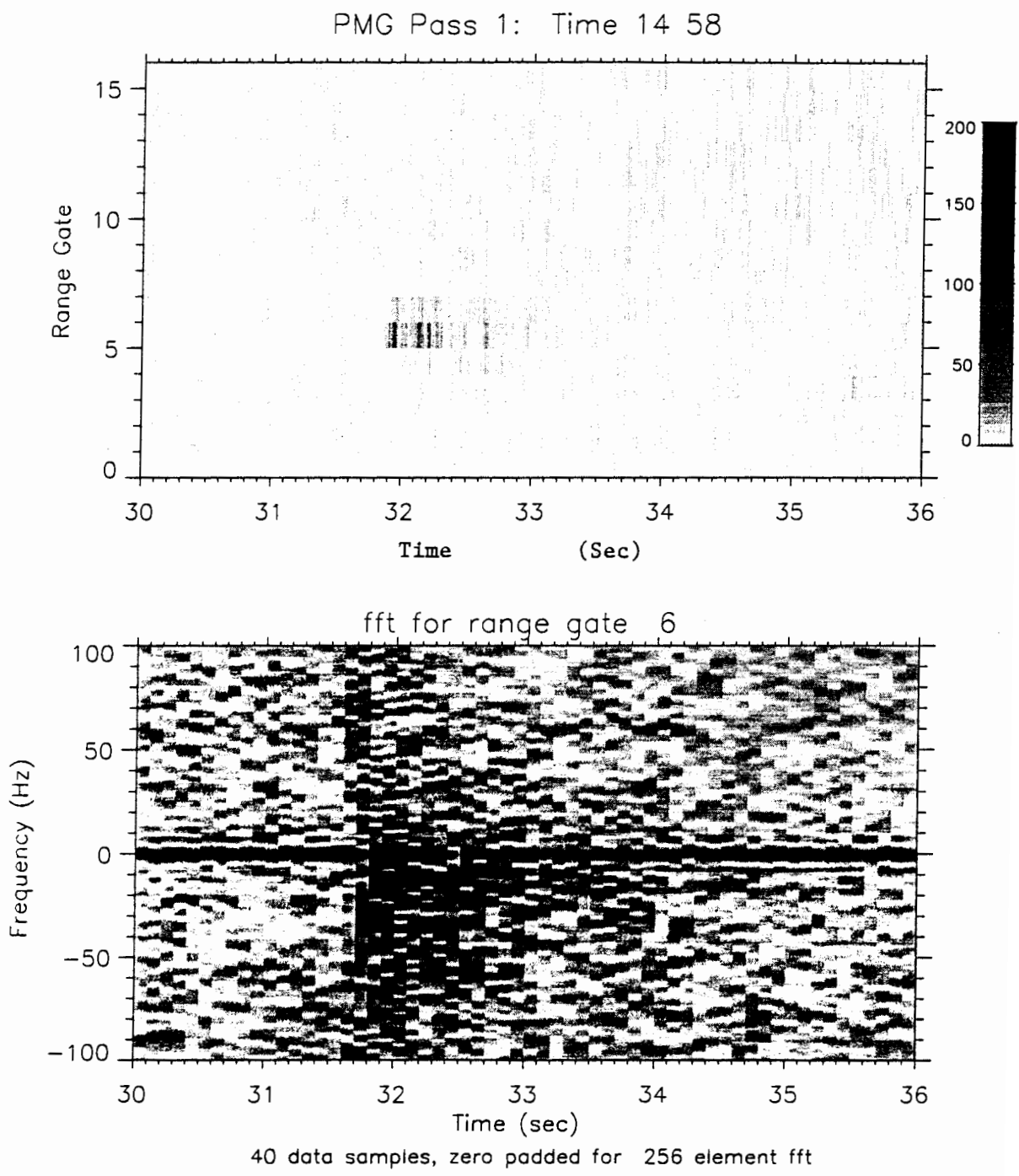


Figure 15. Plasma - Range Gates vs. Time and Spectrogram

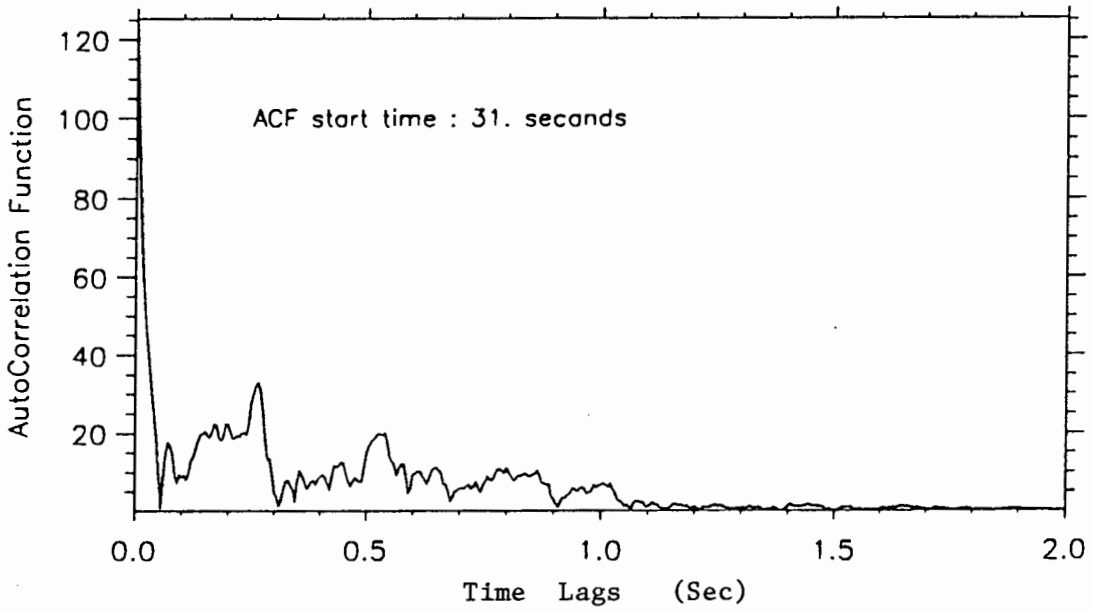
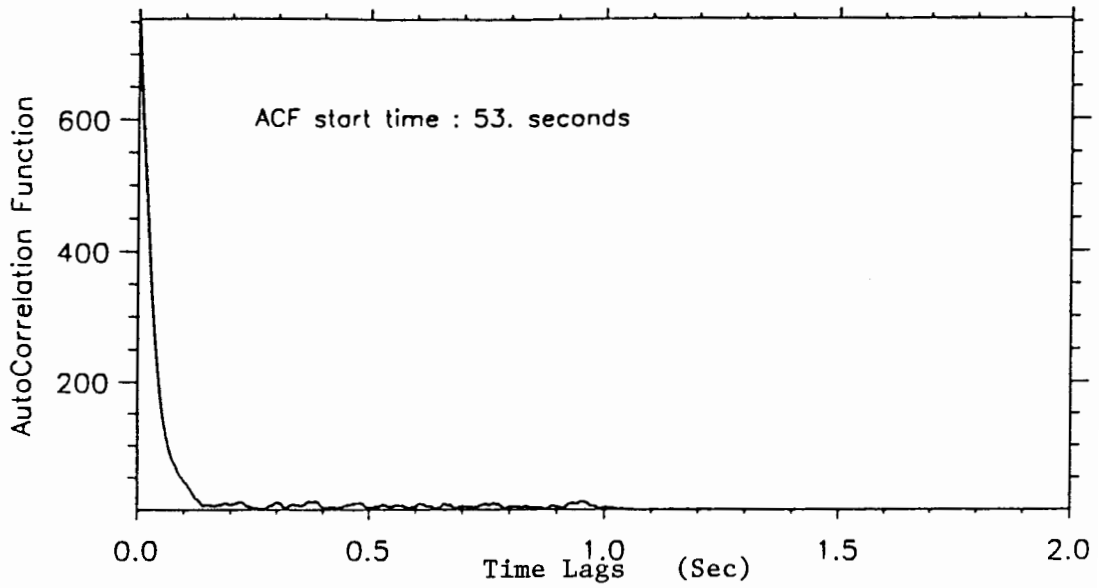


Figure 16. Autocorrelation Fn. - Meteor and Plasma

PMG Pass 1: Time 14 52

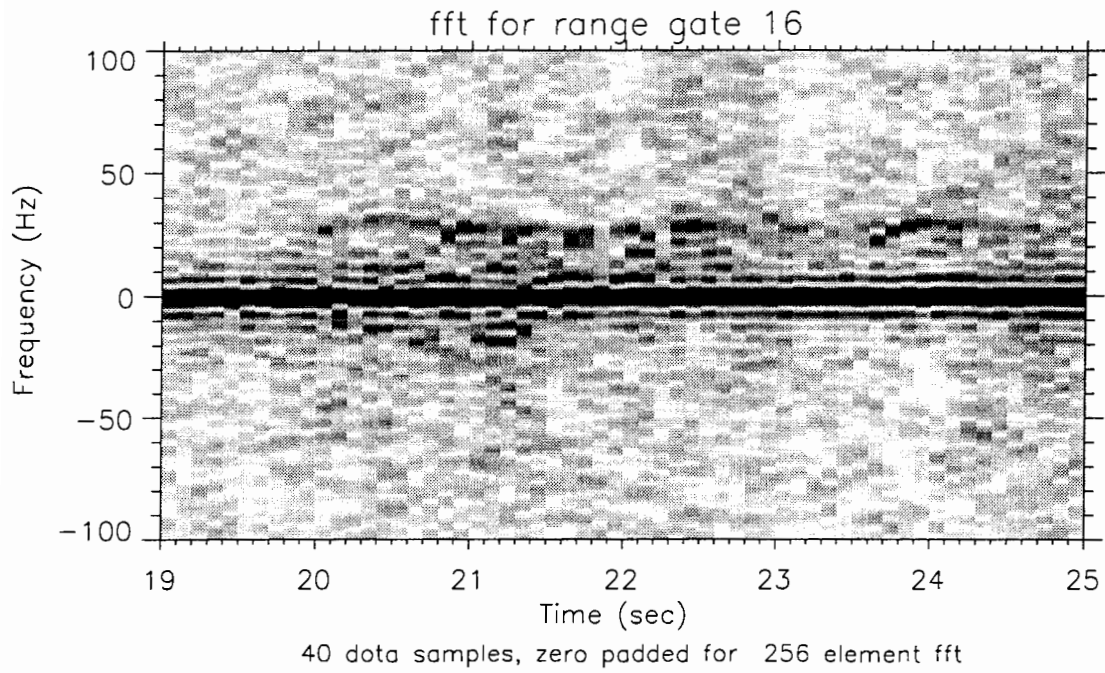
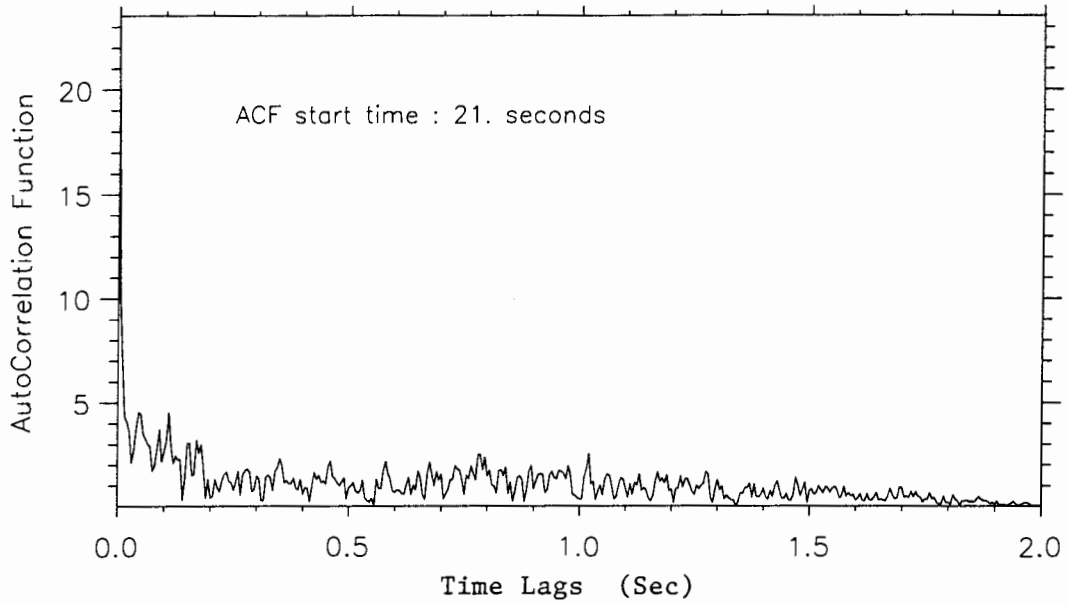


Figure 17. Spectrogram and Autocorrelation Function pass 1, Range Gate 16, Min. 52

PMG Pass 1: Time 14 52

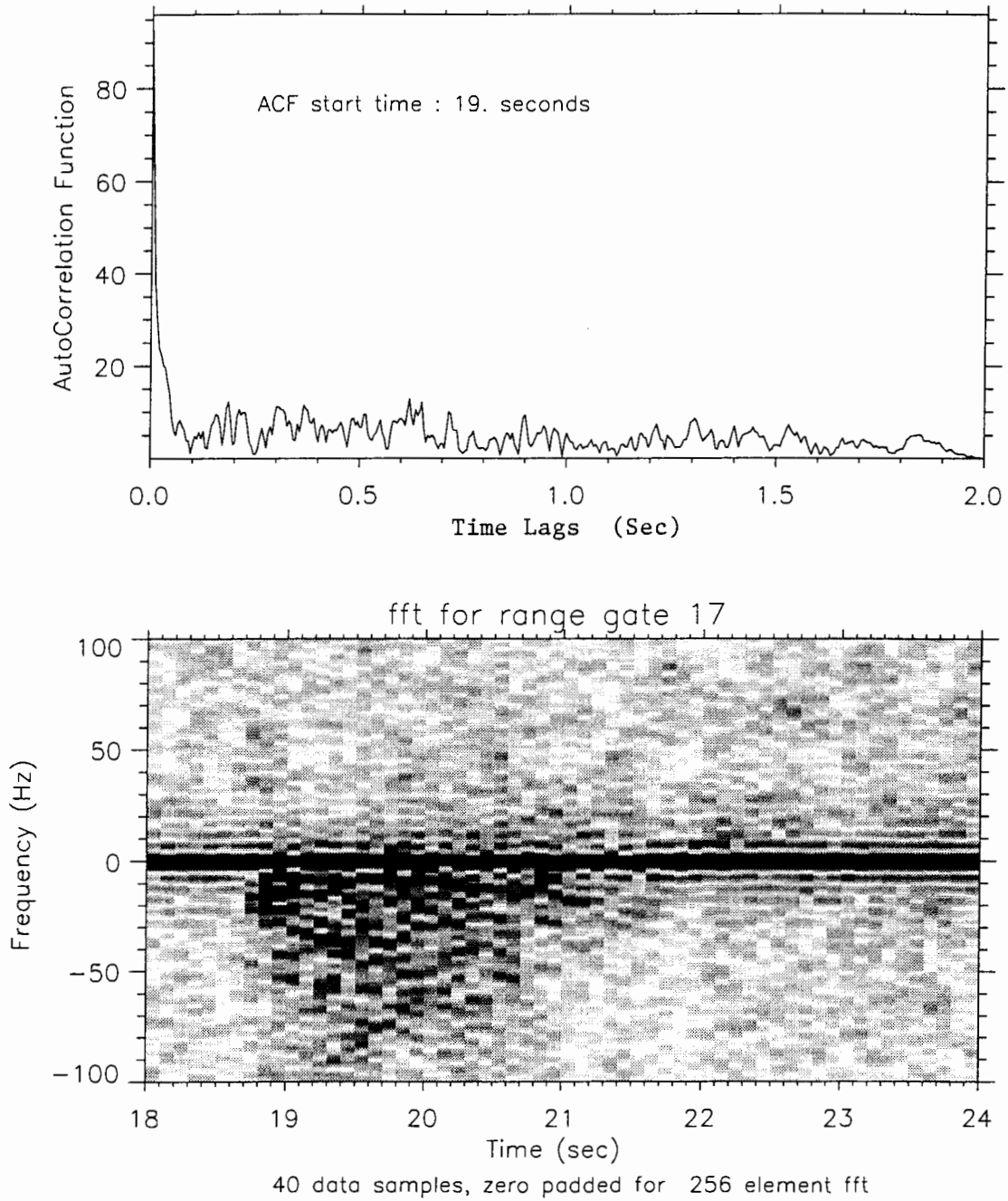


Figure 18. Spectrogram and Autocorrelation Function pass 1, Range Gate 17, Min. 52

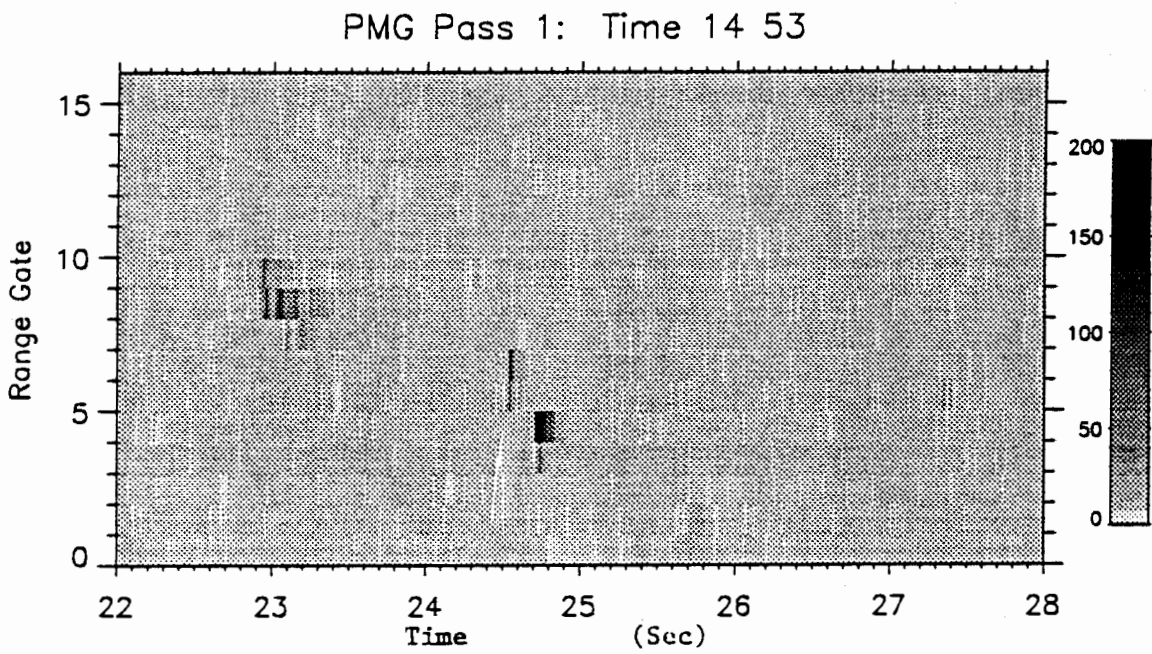


Figure 19. First 16 Range Gates vs. Time From Pass 1, Min. 53

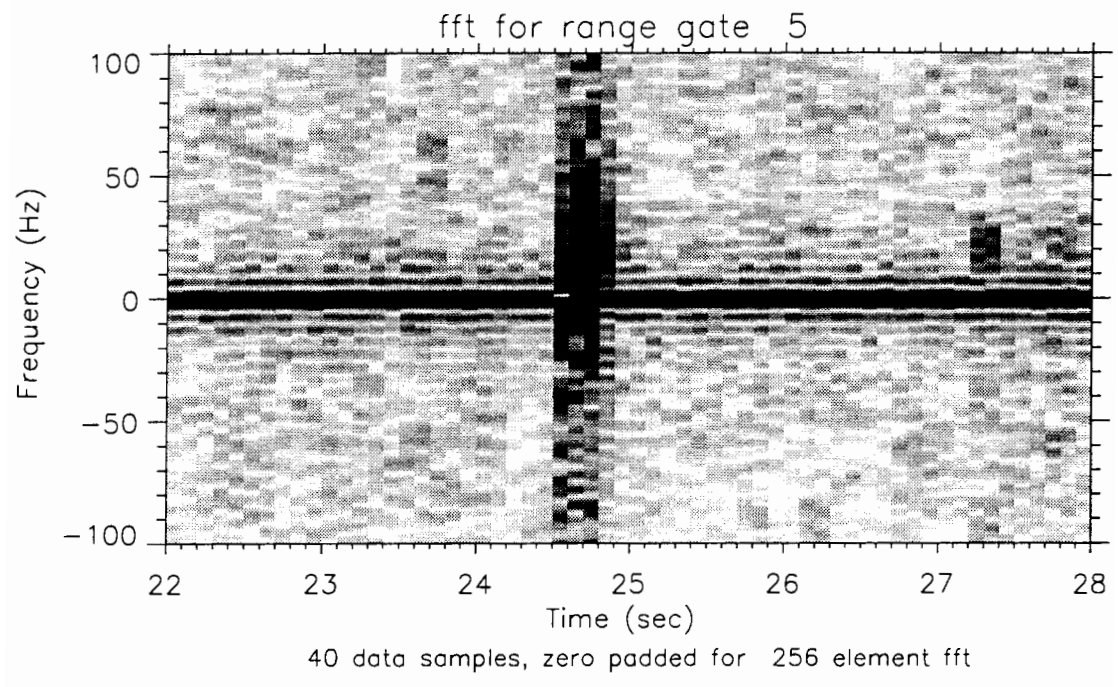
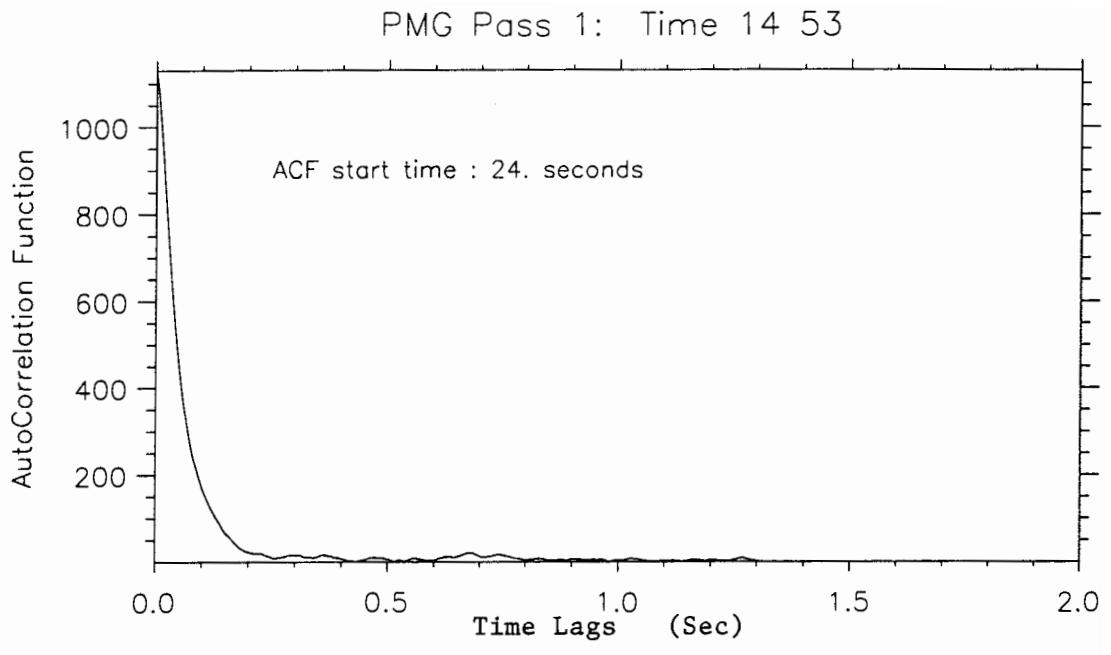


Figure 20. Spectrogram and Autocorrelation Function  
Pass 1, Range Gate 5, Min. 53

PMG Pass 1: Time 14 53

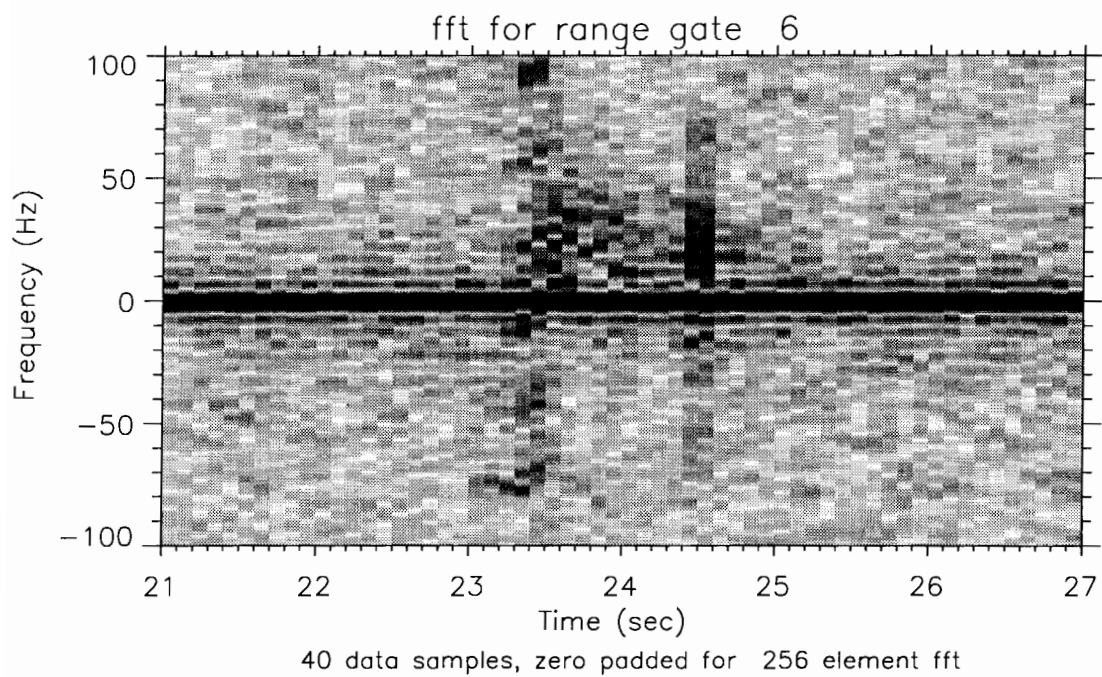
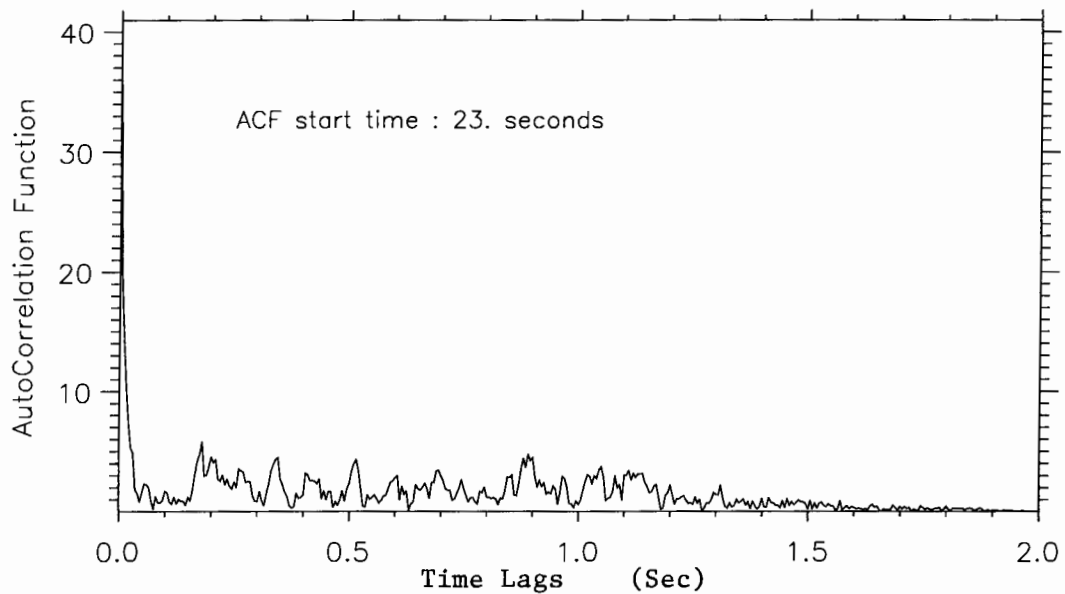


Figure 21. Spectrogram and Autocorrelation Function  
Pass 1, Range Gate 6, Min. 53

PMG Pass 1: Time 14 53

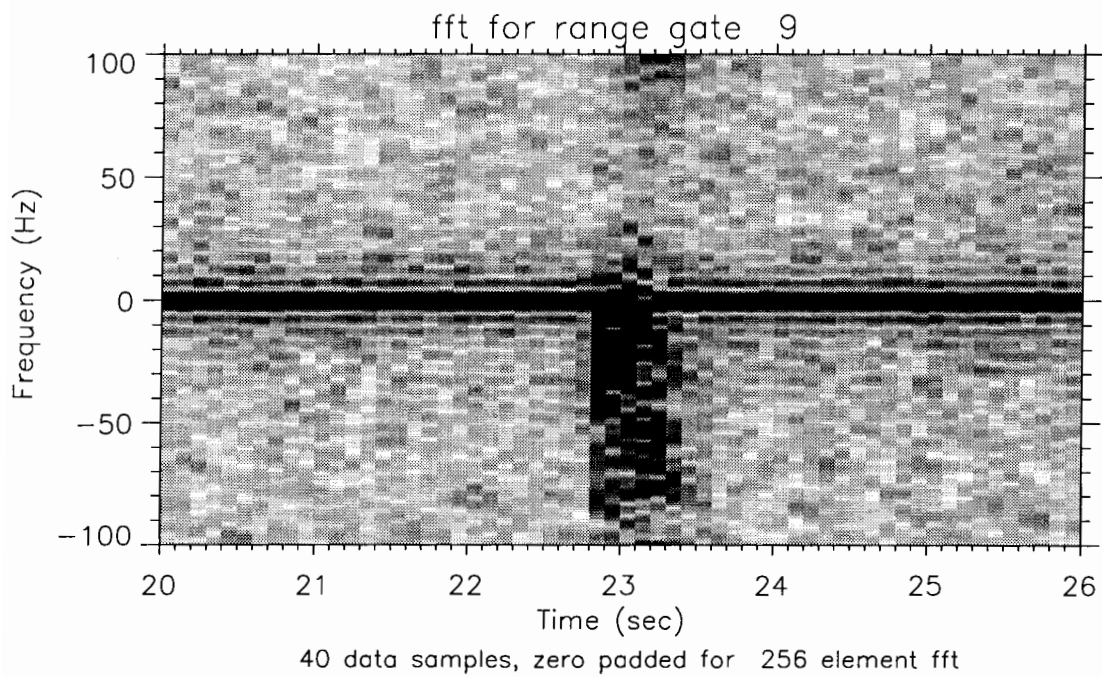
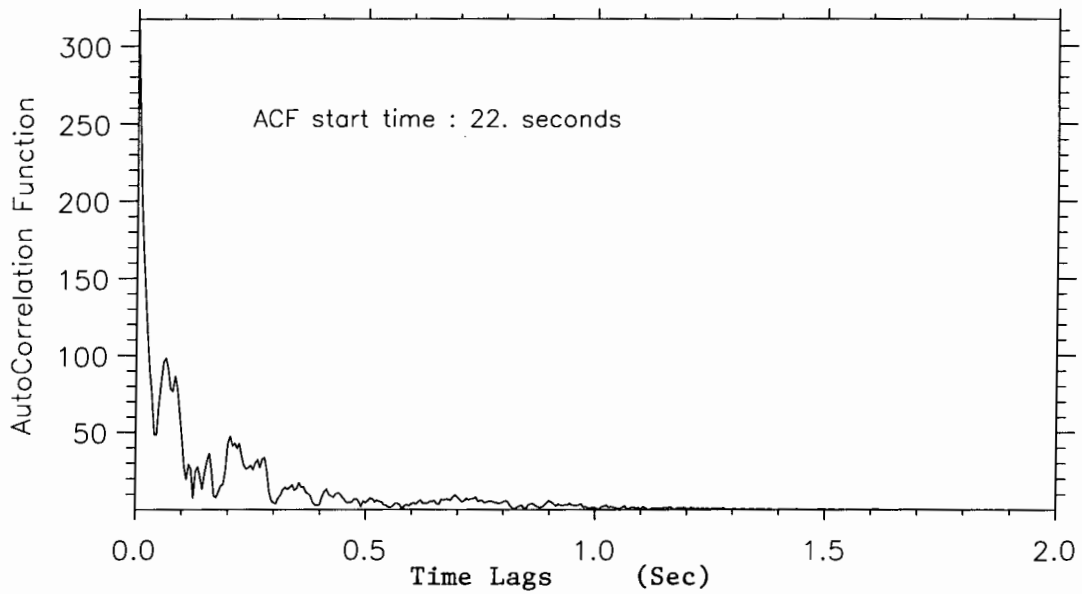


Figure 22. Spectrogram and Autocorrelation Function  
Pass 1, Range Gate 9, Min. 53

PMG Pass 1: Time 14 56

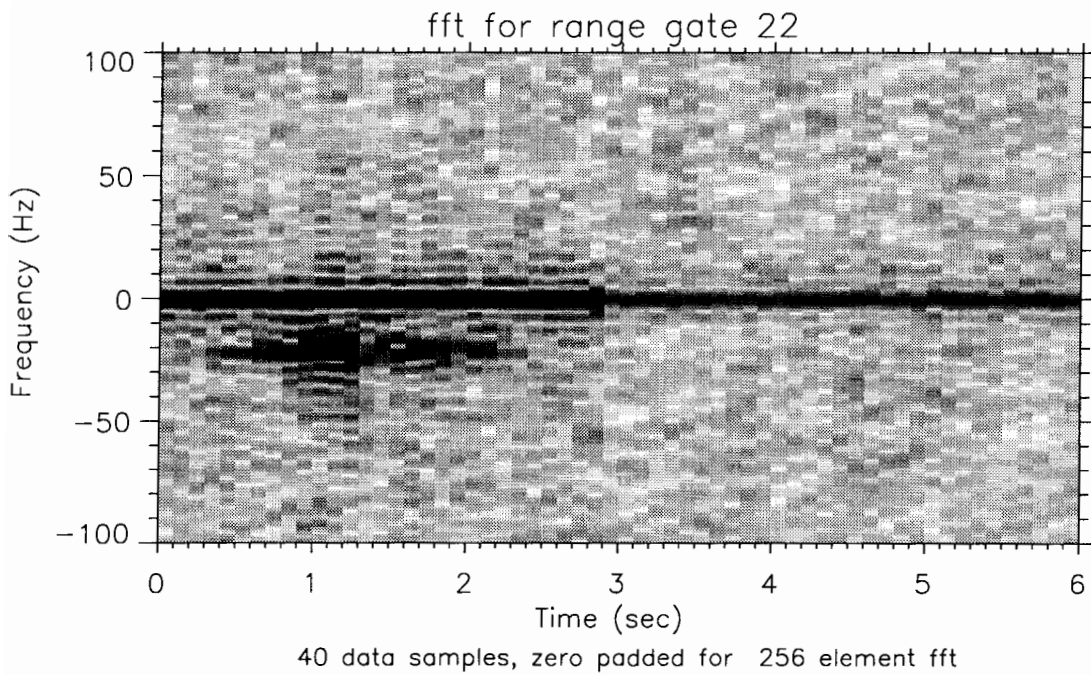
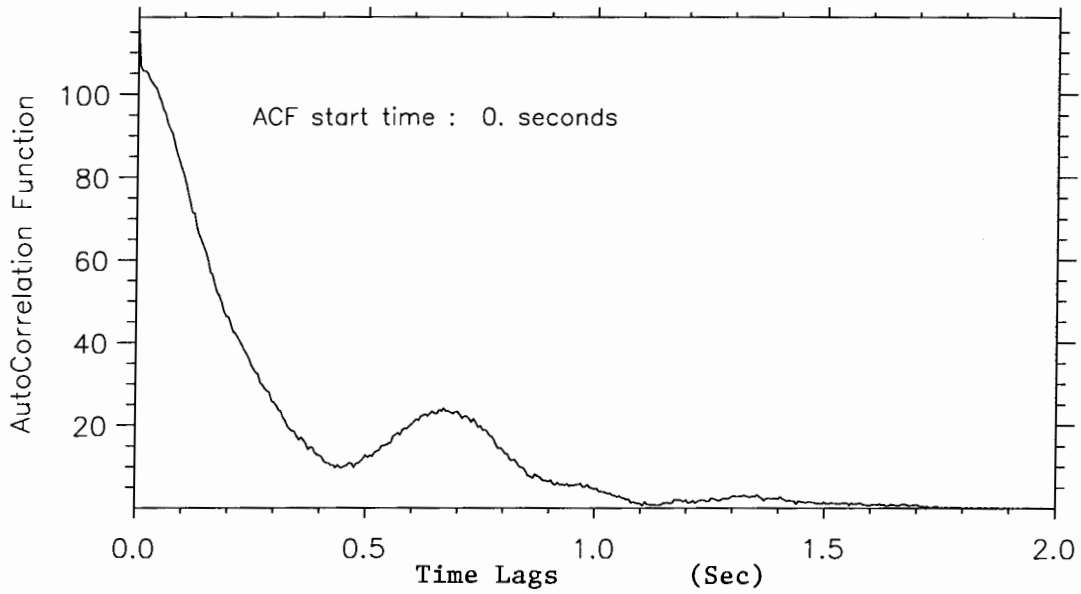


Figure 23. Spectrogram and Autocorrelation Function  
Pass 1, Range Gate 22, Min. 56

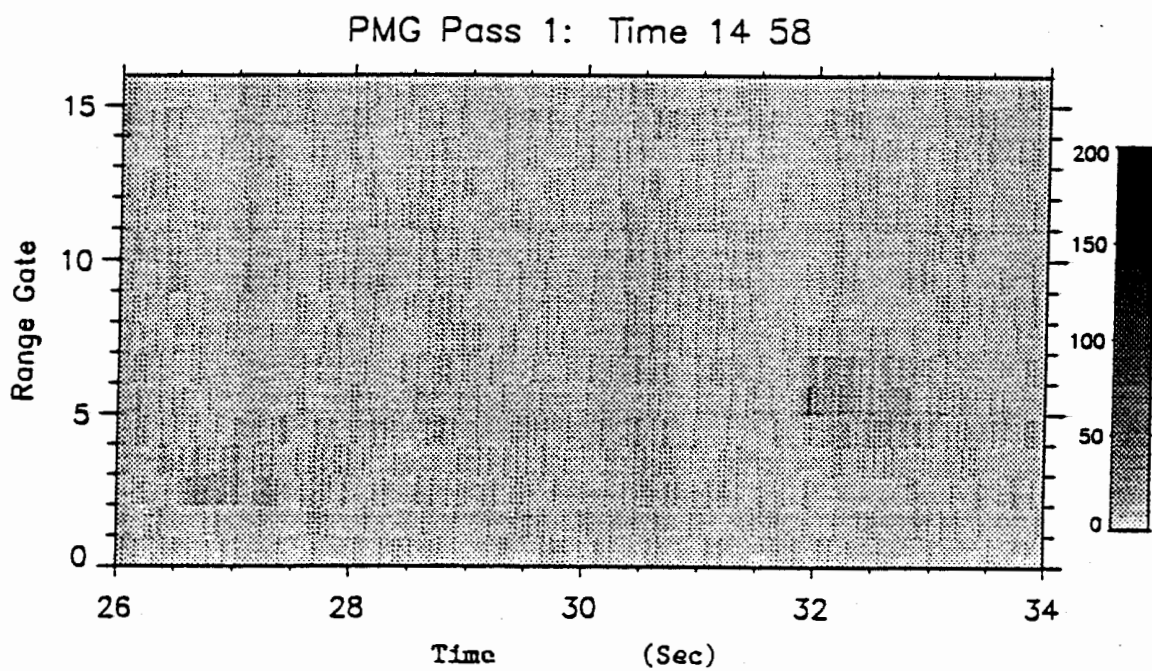


Figure 24. First 16 Range Gates vs. Time From Pass 1, Min. 58

PMG Pass 1: Time 14 58

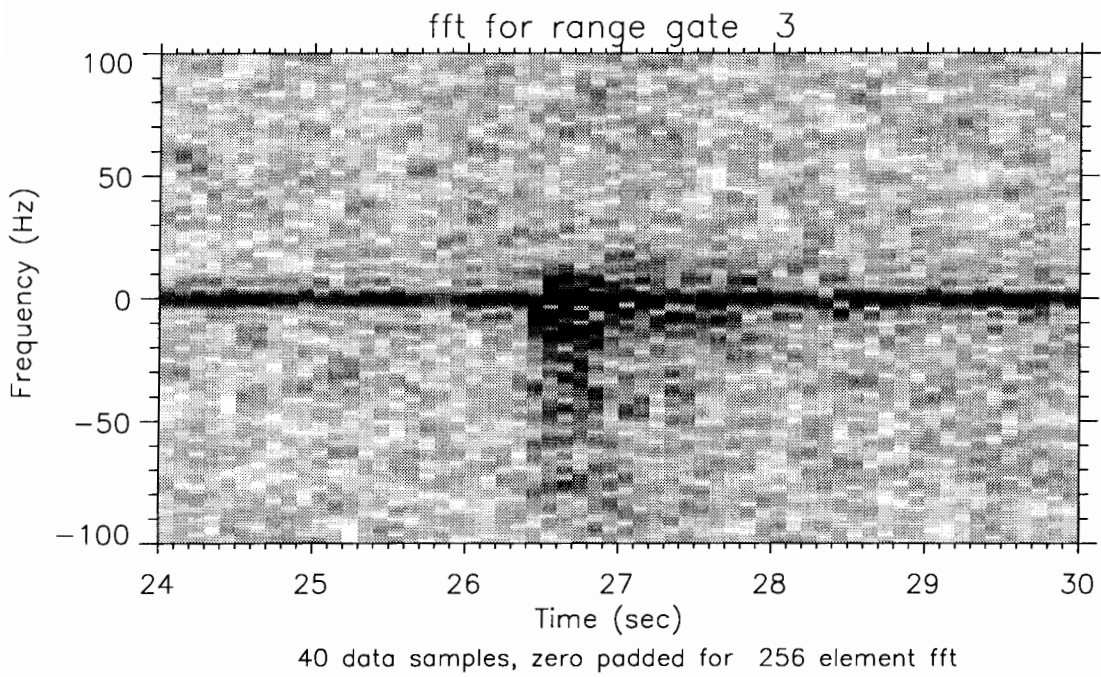
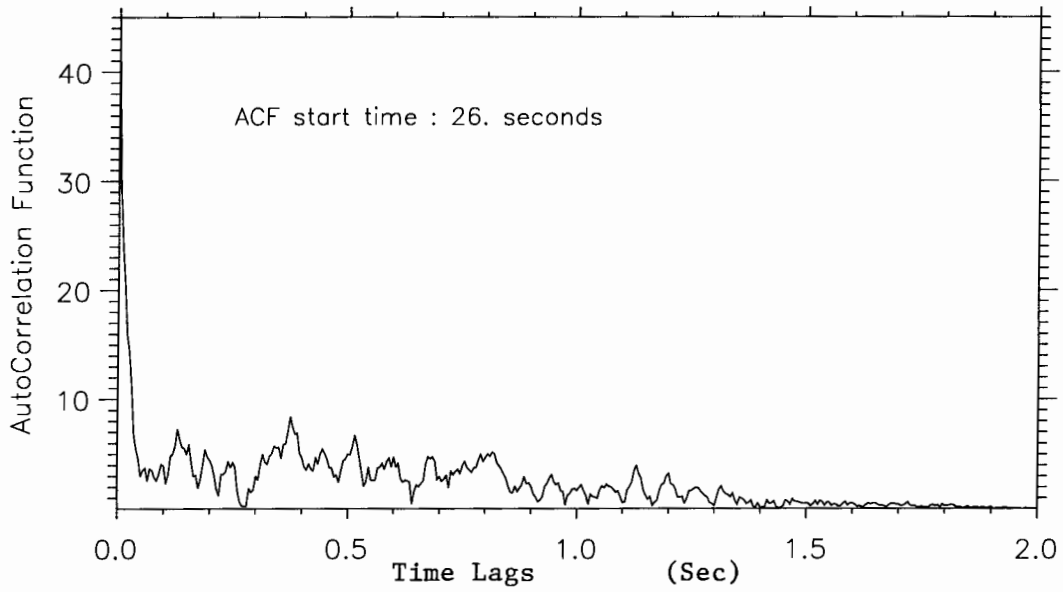


Figure 25. Spectrogram and Autocorrelation Function  
Pass 1, Range Gate 3, Min. 58

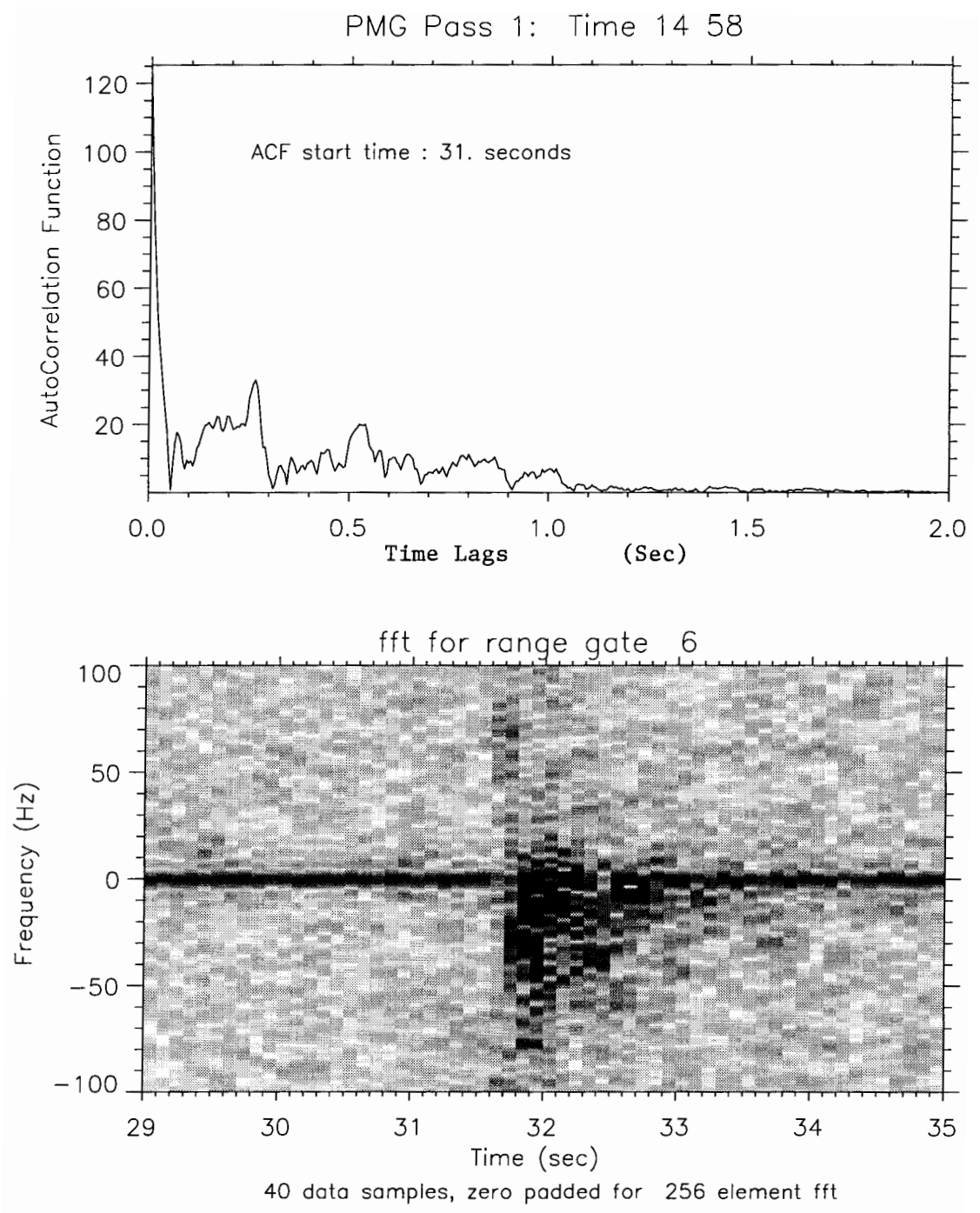


Figure 26. Spectrogram and Autocorrelation Function  
Pass 1, Range Gate 6, Min. 58

PMG Pass 2: Time 16 34

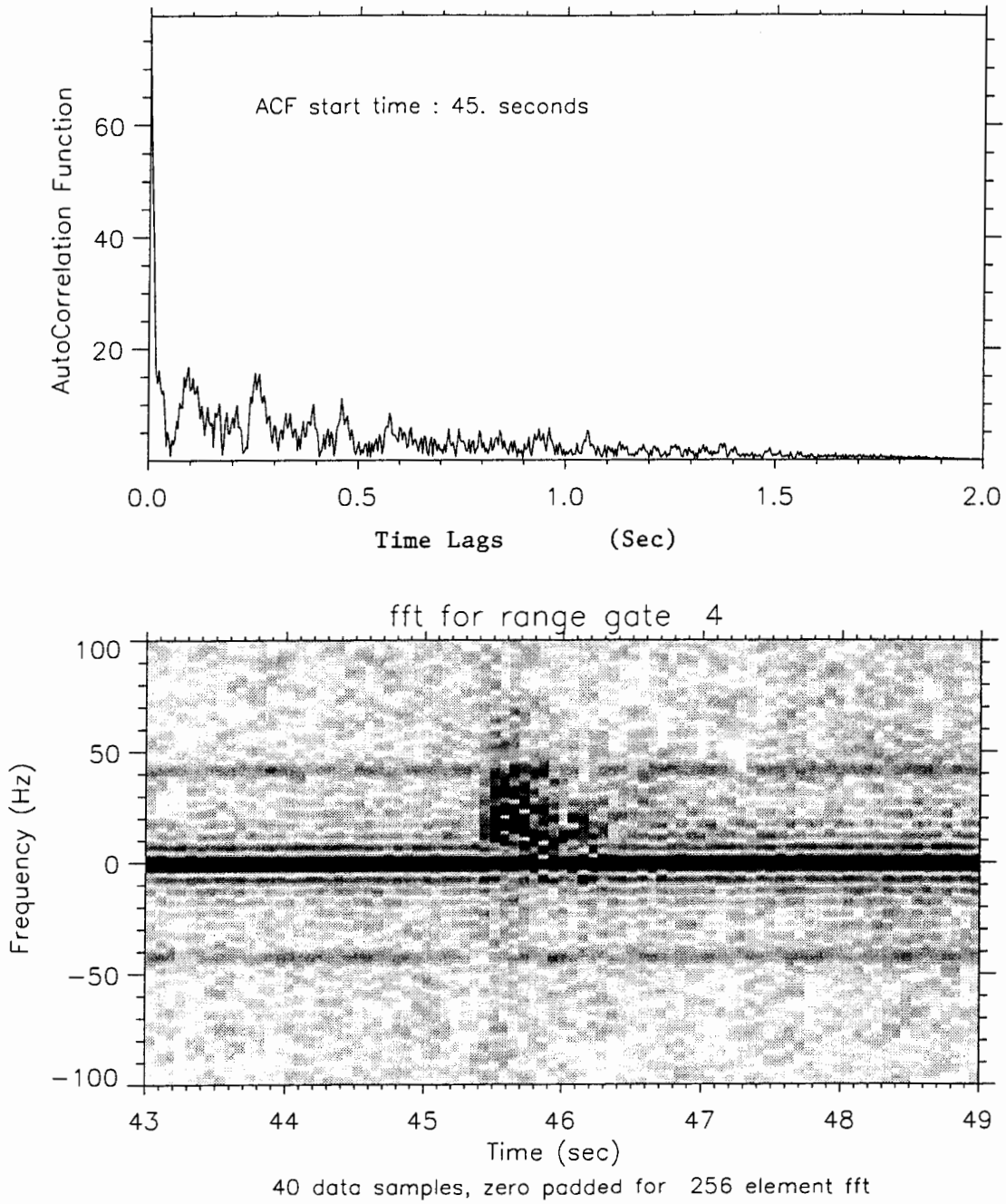


Figure 27. Spectrogram and Autocorrelation Function  
Pass 2, Range Gate 4, Min. 34

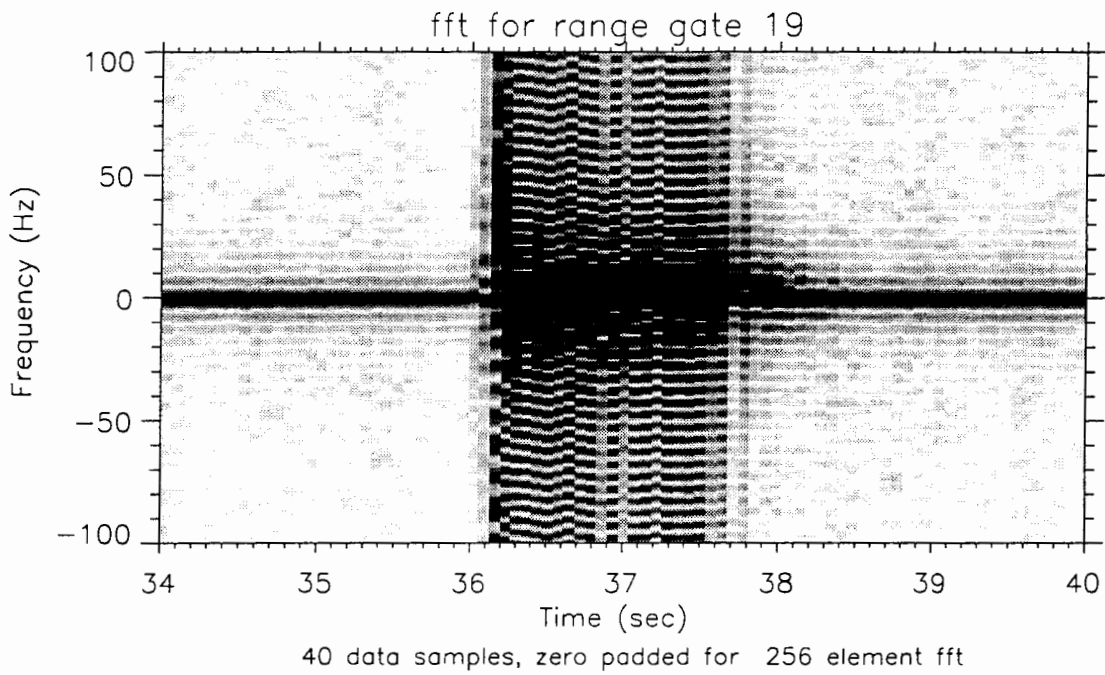
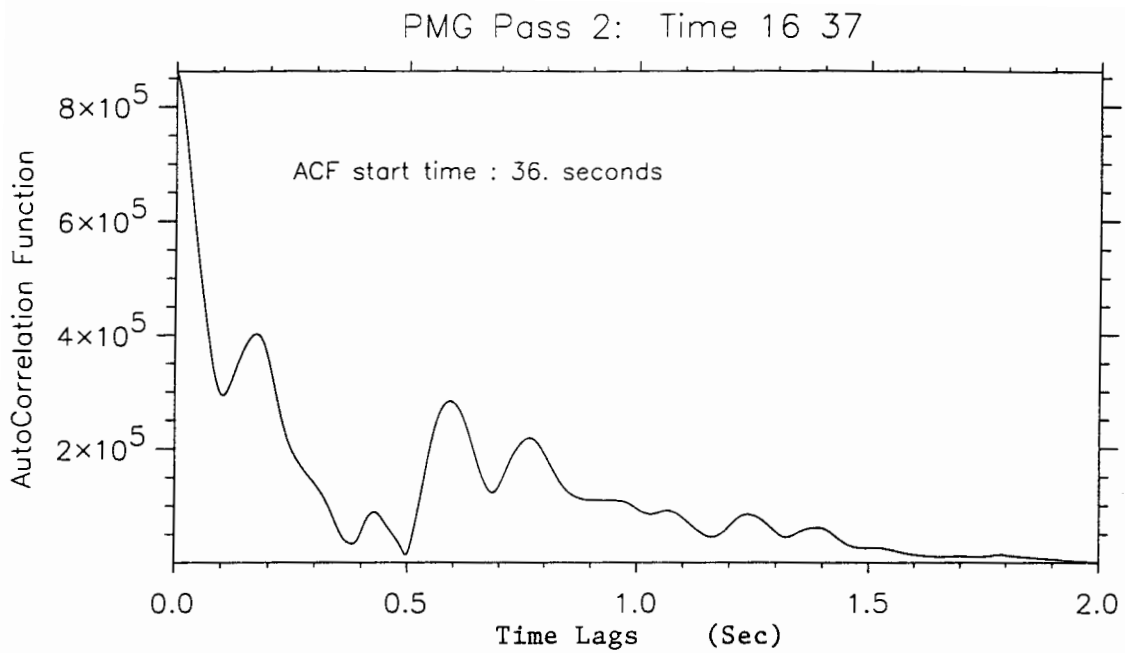


Figure 28. Spectrogram and Autocorrelation Function  
Pass 2, Range Gate 19, Min. 37

## APPENDIX. IDL PROGRAMS

```
*****
*   THIS PROGRAM CALCULATES AND PLOTS THE
*   SPECTROGRAM AND THE 16 RANGE GATES VS.
*   TIME FOR A SELECTED TIME.
*   INPUT VARIABLES REQUIRED:
*       GATE - DEFINES RANGE GATE OF INTEREST
*       BEGIN_TIME - USED FOR START OF SPECTROGRAM
*       END_TIME - USED FOR END OF SPECTROGRAM
*       NUM_SAMPLES - RECTANGULAR WINDOW SIZE
*       FFT_SIZE - SIZE OF FFTs TO BE TAKEN

pro idl_setup, x_win_size, y_win_size, num_colors, ps_or_x

x_win_size = 600.*1. & y_win_size = 800 *1.0& num_colors = 256

ps_or_x = 'x'
ps_or_x = strupcase(ps_or_x)

ps_or_x = 'X' ; initialize for 8 bit display
set_plot, 'x'
device, retain =2, pseudo_color = 8
window, 1, xsize = x_win_size, ysize = y_win_size,
colors = num_colors
loadct, 13 ; 13 for color, use 0 for b&w
tv!ct, r, g, b, /get
r(0) = 255 & g(0) = 255 & b(0) = 255
tv!ct, r, g, b
!p.color = 1

circle = 2*!pi*findgen(9)/8.
radius = 0.2
usersym, radius*cos(circle), radius*sin(circle), /fill

return
end

*****

pro do_plot, title_string, array_of_yfrm, data2, begin_time,
end_time,igate, ps_or_x

x1 = 0.1

image = bytscl(array_of_yfrm, min =0, max = .75, top = 254)
image2 = bytscl(data2, min =0, max = 200, top = 254)
```

```

if ( ps_or_x eq 'X' ) then begin
tv, congrid( image, 60*8, 256), x1*600, .15*800
tv, congrid( image2, 480, 256), x1*600, .6*800
endif else begin
    tv, 254-congrid( image, 60*8, 256), x1*6, .15*8,$
        xsize = 4.8, ysize = 2.56, /inches
    tv, 254-congrid( image2, 480, 256), x1*6, .6*8, $
        xsize = 4.8, ysize = 2.56, /inches
endelse

y1 = .15
x2 = x1 + 60.*8./600.
y2 = y1 + 256./800.
posit = [x1, y1, x2, y2]

plot, image, /nodata, xrange = [begin_time, end_time], /noerase, $
    xtitle = 'Time (sec)!n ', $
    ytitle = ' Frequency (Hz)', $
    yrange = [-100,100], $
    title = 'fft for range gate '+ string(igate + 1, "(i2)")+'!n ' , $
    xstyle = 1, ystyle = 1, yticklen = -.02, xticklen = -.02, $
    position = posit, /normal

second plot.....

y1 = .6
y2 = y1 + 256./800.
posit = [x1, y1, x2, y2]

plot, image2, /nodata, xrange = [begin_time, end_time], /noerase, $
    xtitle = ' ', $
    ytitle = 'Range Gate', $
    yrange = [0,16], $
    xstyle = 1, ystyle = 1, yticklen = -.02, xticklen = -.02, $
    position = posit, /normal, $
    title = title_string

return
end
***** main program here *****

dir = '/sun_data/pmg/pass1/'
file = 'mp114581.bin'

openr, 2, dir+file
day = 177
hour = 14
min = 52
sec = 0.002

```

```

size = 12000
sec = fltarr(size)
s = .002
i = intarr(16, size)
q = intarr(16, size)
data1 = intarr(16)
data2 = intarr(16)
!p.psym = -8
index = 0

print, 'reading in data from ', file

while not eof(2) do begin
  forrd, 2, hour, min, s, data1, data2
  sec(index) = s
  i(0:15,index) = data1(0:15)
  q(0:15,index) = data2(0:15)
  if index eq 1 then start_hour = hour
  if index eq 1 then start_min = min
  index = index+1
endwhile
close, 2

print, 'data read in '

time =sec
igate = 3
gate = 3

read, 'enter range gate for fft spectrogram (1-16) ', gate
igate = gate - 1

print, index, ' data points in array'

j = complex(0,1)

data = i(igate,*) + j*q(igate,*)
; 5 ms per sample

begin_time = 0
end_time = 60
read, 'enter begin_time (0), end_time(60) ', begin_time, end_time
number_seconds = end_time - begin_time

loop_here:
num_samples = 256
read, 'enter number of data samples per fft (256) ', num_samples
fft_size = 256

```

```

read, 'enter number of of steps in fft (256) ', fft_size
if (fft_size lt num_samples) then goto, loop_here

num_steps = 2*(number_seconds * 200) /num_samples
; 2* to do overlap
help, num_steps, num_samples

data_256 = data(0:fft_size-1)
data_256(*) = complex(0.)

starting_step = 2*(begin_time*200)/num_samples
help, starting_step

array_of_yfrm = fltarr(num_steps,fft_size)

for istep = 0, num_steps-1 do begin
  istart = 0.5* (istep+starting_step)*num_samples
  ; 0.5* to do overlap
  finish = istart + num_samples - 1
  if (finish gt index) then goto, skip

  if ( num_samples eq fft_size ) then begin
    time_series = data(istart:finish)
  endif else begin
    time_series = data_256
    time_series(0:num_samples-1) = data(istart:finish)
  endelse

  xfrm = fft( time_series, -1)
  yfrm = abs(xfrm)
  yfrm = shift(yfrm, (fft_size/2)-1 )
  array_of_yfrm (istep,0:fft_size-1) = yfrm(0:fft_size-1)
endfor

skip:
x = indgen(256) - 127

range0 = 200* begin_time
range1 = 200* end_time -1

data2 = abs( i(*, range0:range1) + j*q(*, range0:range1) )
help, data2
direction = 4 ; transpose only x => y, y=> x
data2 = rotate( data2, direction)
help, data2

```

```

; initialize system
idl_setup, x_win_size, y_win_size, num_colors, ps_or_x
title_string = '!A' + 'PMG Pass 1: Time '
+ string( start_hour, start_min, $
"(i2,1x,i2)") + '!n '

do_plot, title_string, array_of_yfrm, data2, begin_time,
end_time, igate, ps_or_x

stop, 'enter .con for postscript plot '

set_plot, 'PS'
device, file='spec.ps', /portrait, $
bits_per_pixel=8, /close_file, /inches, yoffset = 2.0,
ysize = 8.0,$
xoffset = 1.5, xsize = 6.0

loadct, 0
!p.color = 1
ps_or_x = 'P'
do_plot, title_string, array_of_yfrm, data2, begin_time,
end_time, igate, ps_or_x

colbar = bindgen(256)
colbar = reform(colbar, 1,256)
tv, 255-colbar, 5.75, 5.0 , xsize = .2, ysize = 2, /inches
plot, colbar, /nodata, xrange = [0,1], xticks = 1,
xtickname = [' ', ' '], $
yrange = [0,200], ystyle = 1, xticklen = 0.01, yticklen = -.05,$
/noerase, position = [ 5.75/6.0, 5.0/8.0, 5.95/6.0, 7.0/8.0],
/normal, $
charsize = 0.7

lable = string(num_samples,"(i4)") + ' data samples,
zero padded for '
lable2 = string(fft_size, "(i4)") + ' element fft'
xyouts, .2, .07, lable+lable2, size = .9, /normal, color = 1
;xyouts, .2, .01, 'Naval Postgraduate School - Run on '+!stime,
/normal

if (ps_or_x eq 'P') then begin
device, /close_file
endif

set_plot, 'x'

end

```

THIS PROGRAM CALCULATES THE BIASED AUTOCORRELATION FUNCTION  
REQUIRED OPERATOR INPUT VARIABLES ARE:

r11 - autocorrelation start time in seconds; and  
e11 - autocorrelation end time in seconds.

```
pro auto_corr, x, range, acf, bias
    ; x is a one-d array, range is a2 element vector
    ; defining subset of x you want to autocorrelate
    ; acf is the autocorrelation function we return,
    ; a vector bias is flag for biased vs unbiased acf

bias = 1; do biased - each element divided by number
    ; of elements selected for acf

x1 = x( range(0): range(1) )
x2 = conj (x1)          ; the complex conjugate
                        ; have assumed at this point data are
                        ; in complex

n_ele = 1+ range(1) - range(0)
acf = complexarr(n_ele)

acf(0) = total(x1*x2)
for i = 1, n_ele -1 do begin
x2 = shift(x2, 1)
x2(0) = 0
acf(i) = total(x1*x2)
endfor

acf = acf/n_ele          ; assume bias = 1 for now

return
end

read, 'enter ACORR start time',r11
r1=r11*200
read,'enter ACORR end time',e11
e1=e11*200
range= [1,r1:e1 ]
auto_corr, x, range, acf, bias
plot, acf & wait, 1
end
```

## LIST OF REFERENCES

Edde, B., *Radar Principles, Technology, Applications*, Prentice Hall, New York, NY, 1993.

Jost, R.J., *Ground-Based Ionospheric Sensor Observations*, NASA/JSC Technical Report #JSC26511, Houston TX, 1994.

NASA, *Tethers in Space Handbook*, NASA Headquarters, Code MD, Conference Proceedings, Washington, DC, 1986.

Olson, D.M., "Radar Observations of Field-Aligned Plasma Propagations Associated with NASA's PMG Experiment," Master's Thesis, Naval Postgraduate School, September, 1994

Penzo, P.A., "Tethers for Mars Space Operations," *Astronautics and Aeronautics, Journal*, 1984.

Skolnik, M.I., *Introduction to Radar Systems*, McGraw-Hill, Inc., New York, NY, 1980.

Swords, S.S., *Technical History of the Beginnings of Radar*, IEEE History of Technology Series, vol. 6, Peter Peregrinus Ltd., London, United Kingdom, 1986.

Tennekes, H. and Lumley, J.L., *A First Course in Turbulence*, The MIT Press, Cambridge, MA, 1974.



### INITIAL DISTRIBUTION LIST

|    |   |   |
|----|---|---|
| 1. | Defense Technical Information Center .....        | 2 |
|    | Cameron Station                                   |   |
|    | Alexandria, Virginia 22304-6145                   |   |
| 2. | Library, Code 52 .....                            | 2 |
|    | Naval Postgraduate School                         |   |
|    | Monterey, California 93943-5101                   |   |
| 3. | Chairman, Code PH .....                           | 1 |
|    | Department of Physics                             |   |
|    | Naval Postgraduate School                         |   |
|    | Monterey, California 93943-5117                   |   |
| 4. | Chairman, Code EC .....                           | 1 |
|    | Department of Electrical and Computer Engineering |   |
|    | Naval Postgraduate School                         |   |
|    | Monterey, California 93943-5121                   |   |
| 5. | Prof. Ralph Hippenstiel, Code EC/Hi .....         | 1 |
|    | Department of Electrical and Computer Engineering |   |
|    | Naval Postgraduate School                         |   |
|    | Monterey, California 93943-5121                   |   |
| 6. | Prof. R.C. Olsen, Code PH/Os .....                | 5 |
|    | Department of Physics                             |   |
|    | Naval Postgraduate School                         |   |
|    | Monterey, California 93943-5117                   |   |
| 7. | Dr. R.J. Jost .....                               | 2 |
|    | System Planning Corporation                       |   |
|    | 18100 Upper Bay Road                              |   |
|    | Houston, Texas 77058                              |   |
| 8. | D.M. Olson .....                                  | 1 |
|    | 210 Meadowlark Lane                               |   |
|    | Duncanville, Texas 75137                          |   |

|     |  |         |
|-----|--|---------|
| 9.  | Dr. Jim McCoy<br>NASA/JSC, Code SN3<br>Houston, Texas 77058  | ..... 2 |
| 10. | Dr. Nobie Stone<br>NASA/Marshall SFC, Code ES53<br>Huntsville, AL. 35812   | ..... 1 |
| 11. | Dr. Mario Grossi<br>Smithsonian Institution Astrophysical Observatory<br>Cambridge, MA. 02138  | ..... 1 |
| 12. | Professor Lucca Minna<br>Department of Biophysical and Electronic Engineering<br>University of Genoa<br>Via all'Opera Pia 11A  | ..... 1 |
| 13. | Professor M. Dobrowolny<br>Consiglio Nazionale delle Ricerche<br>Istituto di Fisica Dello, Spazio Interplanetario<br>Via G. Galilei, Casella Postale 27<br>I-00044 Frascati, Italy | ..... 1 |
| 14. | Commander, Naval Space Command<br>ATTN: N112<br>5280 4th Street<br>Dahlgren, VA. 22448-5300  | ..... 1 |
| 15. | W. A. Brewster<br>RR #2 Albert<br>New Brunswick, Canada, EOA 1A0   | ..... 2 |



